[illegible] COEFFICIENT AND ELECTRICAL RESISTIVITY [illegible] CIRCUIT CHARACTERISTICS

Edmund Y. M. Lee

A MAJOR TECHNICAL REPORT

in the

Faculty of Engineering

Presented in partial fulfillment of the requirements for
the Degree of Master of Engineering at
Sir George Williams University
Montreal, Canada

April, 1974

TABLE OF CONTENTS

LIST OF FIGURES

LIST OF TABLES

HALL COEFFICIENT AND ELECTRICAL RESISTIVITY

[illegible] OF MERCURY CHALCOGENIDES

Edmund Y. M. Lee

ABSTRACT

Mercury telluride, selenide and their alloys ($HgTe_{1-x}Se_x$) were prepared by the modified Bridgeman technique. Hall coefficient and electrical resistivity measurements were performed on these crystals from 1.5°K to 350°K. In the case of mercury telluride, a p- to n-type transition was observed at 53.4°K. This curve was fitted by using an inverted two-carrier model for the entire investigated temperature range. The best fit of the experimental curve was obtained with a thermal energy gap $E_t = 0 \pm .001$ ev.

The other alloys containing increasing amount of selenium ($\Delta x = 0.2$) were n-type. Attempts were made to investigate the Hall coefficient curves of the mercury chalcogenide alloys. The results seem to indicate that in these cases the two-carrier model fails since the energy gap $E_g = E_{\Gamma_6} - E_{\Gamma_8}$ decreases to such an extent that the deep lying light holes cannot be neglected any more.

ACKNOWLEDGEMENTS

I would like to express my sincere thanks to my research supervisor, Dr. B. A. Lombos, for his guidance, encouragement and cooperation during the course of this work.

I would like to thank Dr. A. Kipling of the Physics Department for giving me the privilege of working in the Low Temperature Measurement Laboratory where the measurement part of this work was carried out.

Thanks are also due to Mr. R. Krawczynuik for his assistance in taking Hall effect measurements; to Mr. N. Yemanidjian for his help in computer programming and to Mrs. A. Margittai for her help in the Microelectronics Laboratory.

CHAPTER I

INTRODUCTION

Narrow energy gap semiconductors have been extensively studied since many years. One of the reasons is because of their potential as an intrinsic infrared detector. An intrinsic infrared detector is basically a very simple semiconductor device. When infrared radiation is incident on the device the electrons are excited from states near the top of the valence band into states at the bottom of the conduction band causing excess electron-hole pairs. These change the electrical properties of the material in the form of electrical conductivity. The cutoff wavelength of the device is related to its energy gap by

$$E_g = \frac{h c_o}{\lambda} \qquad (I\text{-}1)$$

where E_g is the energy gap width of the material, h is the Planck's constant, c_o is the velocity of light and λ is the cutoff wavelength. Expressing E_g in electron-volt (ev) and λ in micro-meter (μm) equation (I-1) becomes

$$E_g = \frac{1.24}{\lambda} \qquad (I\text{-}2)$$

Existing semiconductor materials having suitable energy gap width for intrinsic infrared detectors cover only a small

portion (1-10 μ) of the infrared wavelength range (1-1000 μm). Thus there is a need for new materials which have wide range of energy gap. One method of achieving this is by alloying two or more semiconductors of different energy gap widths in varying proportions.

This work is the first phase of a research program on infrared detectors, mainly in the wavelength range of 100-1000 μm examining mercury telluride-selenide alloys ($HgTe_xSe_{1-x}$, $0 \leq x \leq 1$). There are quite a number of basic problems which have to be solved in this subject but the scope of this present phase is confined to the study of the band structure and other electrical properties of these alloys - $HgTe_xSe_{1-x}$, $0 \leq x \leq 1$, $x = 0.2$.

In An electron is in a state such that its wavelength is quite different from the spacing between the ion cores along its path, then the effect of the lattice of ions are not drastic. However, the wave is strongly diffracted when the Bragg condition is satisfied:

$$k \sin\theta = \frac{n\pi}{a} \quad n = 1, 2, \ldots \quad (I-3)$$

where $k = \frac{2\pi}{\lambda}$, is the wave number, λ is the wavelength, a is the spacing between adjacent atomic planes, and θ is the angle of incidence. A crystalline solid consists of many sets of lattice planes oriented in different directions, and the regions enclosed by the planes at which Bragg condition is satisfied are known as the Brillouin zones in the reciprocal lattice. Hence the shapes of the Brillouin zones are determined solely by the crystalline structure. The

[illegible] crystallize in [illegible] the [illegible] with the [illegible] vicinity of the center of the Brillouin zone ($\vec{k}=0$) which is characterized by the symmetry operation Γ^1 and where the extrema of the valence and conduction bands occur.

Although mercury telluride (HgTe) has been extensively studied for many years, mostly in connection with the cadmium mercury telluride, any attempt to explain its physical properties presents a formidable task. Earlier investigators like Black et al (1), Harman et al (2) and Lawson et al (3), on the basis of their electrical measurements, estimated HgTe to be a narrow gap semiconductor with energy gap of 0.01–0.025 ev. More recent workers like Verie and Decamp (4), Piotrzkowski et al (5), Stradling (6) and Harman (7), however, favour the inverted band structure similar to that of gray tin (8). On the basis of this model they estimated the energy gap to be -.15 ev at 295°k and was very temperature sensitive. While this inverted band structure model is generally accepted, the values of some band parameters reported by these workers vary greatly, especially the amount of overlapping between the valence and conduction bands E_t ($k\neq 0$) which range from 0 to -0.02 ev. Table I-1 shows some of the band parameter values as reported in literature.

---

[1] Symmetry elements in the character table of the irreducible representation for the diamond and zincblende structure.

The object of this study is by fitting the Hall coefficient versus temperature curve with both the conventional and inverted band models and by comparing these results some of these inconsistancies may be removed. The basic theory necessary to the work presented in this thesis is reviewed in Chapter II. Chapter III describes the experimental apparatus and technique. Chapter IV presents the experimental results and their interpretation and Chapter V contains a conclusion and presents some recommendations.

TABLE I-1

VALUES OF SOME BAND PARAMETERS REPORTED IN LITERATURE

Compound	Energy Gap (ev)		Effective Mass (m_o)		Ref.
	$E_g = E_{\Gamma_6} - E_{\Gamma_8}$	$E_t = E_c - E_v$ ($k \neq 0$)	Electron m_e^* ($k=0$)	Hole m_h^*	
HgTe	0.01				(3)
	0.02				(2)
	0.025				(1)
	-0.30 (4.2°K)	0			(9)
	-0.15 (295°k)				(4,9)
		-.003	.029 (4.2°K)	0.35	(6)
		-.02			(7)
			.027 (4.2°K)		(10,11)
				0.08	(12)
				0.55	(13)
HgSe	-0.19 (4.2°K)				(9)
	-0.08 (295°K)				(9)
	-0.24 (4.2°K)				(14)
	-0.15 (295°K)				(7)
		-0.07		0.17	(15)

CHAPTER II

THEORY

2.1 Hall Effect and Electrical Resistivity

The Hall effect occurs when a current-carrying material is subjected to a magnetic field perpendicular to the direction of the current. The migrating electrons crowd to one side of the material due to the Lorentz force acting on them and thus a potential gradiant is developed across the material. Figure II-1 shows the directions of the anplied current and magnetic field on a parallelpiped sample and the sign convention for the Hall voltage, V_H, is taken as indicated in the drawing. The Hall coefficient R_H is given by

$$R_H = \frac{V_H t}{IB} \times 10^8 \qquad (II-1)$$

where R_H is in cm^3 $coulomb^{-1}$, V_H in volts, I in Amperes, B in Gauss and t, the thickness of the sample, in cm.

Under isothermal condition the Hall coefficient of an isotropic semiconductor can be related to its charge carrier concentrations. Futhermore, R_H is independent of the magnetic field intensity if the weak field condition is satisfied, that is $\mu B \ll 1$, and μ is the mobility of the charge carrier. For the case of two types of charge carriers (electrons and holes) the Hall coefficient is given by

$$R_H = -\frac{r}{e} \cdot \frac{\mu_n^2 n - \mu_p^2 p}{(\mu_n n + \mu_p p)^2} \qquad (II-2)$$

where μ_n, n are the mobility and concentration of the electrons and μ_p, p the corresponding quantities of the hole; and e is the electronic charge. The scattering factor, r, is defined as

$$r = \frac{\langle \tau^2 \rangle}{\langle \tau \rangle^2} \qquad (II-3)$$

where τ is the relaxation time and the mean values, $\langle\ \rangle$, are taken over the Fermi-Dirac distribution function. Letting the mobility ratio to be

$$b = \frac{\mu_n}{\mu_p} \qquad (II-4)$$

equation (II-2) becomes

$$R_H = -\frac{r}{e} \cdot \frac{b^2 n - p}{(bn + p)^2} \qquad (II-5)$$

Hence, for $p \gg n$, R_H is positive; for $n \gg p$, R_H is negative. A reversal of sign of the Hall coefficient occurs at Hall zero where $b^2 n = p$.

For a piece of semiconductor of parallelpiped shape the electrical resistivity, ρ, is given by

$$\rho = \frac{V_x\, t\, w}{I\, x} \qquad (II-6)$$

where V_x is the voltage drop between the two measurement probes, x is distance between them and w is the width of the sample.

[illegible] of the carrier concentrations

$$\rho = \frac{1}{\sigma} = \frac{1}{e(n\mu_n + p\mu_p)} \qquad (II-7)$$

where σ is the electrical conductivity.

The Hall mobility is a frequently used quantity in Hall effect measurement. It is defined as

$$\mu_H = \frac{R_H}{\rho} \qquad (II-8)$$

This quantity has real physical significance only in the case of a one carrier system. For $p \gg n$, equation (II-4) and (II-6) becomes

$$R_H = \frac{r}{pe} \qquad (II-9)$$

and $$\rho = \frac{1}{\mu_p p} \qquad (II-10)$$

hence $$\mu_H = r\mu_p \qquad (II-11)$$

Similarly, for the case when $n >> p$

$$\mu_H = r\mu_n \qquad (II-12)$$

2.2 Carrier Mobility and Scattering Processes

When a weak electric field E is applied to a semiconductor the average drift velocity of a carrier is given by

$$v = \mu E \qquad (II-13)$$

The proportionality constant μ is known as the mobility and,

for parabolic energy bands, is defined as

$$\mu = \frac{e\langle\tau\rangle}{m^*} \qquad \text{(II-14)}$$

where m^* is the effective mass of the carrier. If the energy band is not parabolic the effective mass is a function of energy and hence should be included in the averaging process. Therefore, for non-parabolic energy band

$$\mu = e\left\langle\frac{\tau}{m^*}\right\rangle \qquad \text{(II-15)}$$

When there are more than one scattering mechanism affecting the charge carriers the effective relaxation time τ_e must be used in equations (II-14) and (II-15) to calculate the carrier mobility. The effective relaxation time is given as

$$\frac{1}{\tau_e} = \frac{1}{\tau_1} + \frac{1}{\tau_2} + \cdots \qquad \text{(II-16)}$$

where $\tau_1, \tau_2, \ldots$ are the relaxation times for the different scattering modes.

Because of the complexity of the calculations the derivation of a relaxation time for a particular type of scattering processes is not presented. Instead, the major types of scattering processes are discussed qualitatively. In general, the mobility will be determined at low temperatures by crystal structure defects and impurities, and at high temperatures by vibrations of the lattice. Lattice vabrations are of two types. Acoustic vibrations are those in which an atom of a crystal and its nearby neighbours vibrate in phase. Optical vibrations are those in which two adjacent particles

move in opposite directions (out of phase). Early calculations of mobility by Bardeen and Shockley (16) considered only acoustic-mode scattering. This leads to a mobility which varies as $T^{-3/2}$. Experimentally observed deviations of the mobility from the $T^{-3/2}$ dependence arise from a variety of competing effects, including the non-spherical energy surfaces of some semiconductors and the scattering of the more energetic carriers at higher temperatures by optical phonons.

The presence of impurities in the semiconductor also contributes to the scattering of the charge carriers. Scattering by ionized impurities yields a mobility which varies as $T^{3/2}$ (17,18). An expression for the mobility which results from neutral impurity scattering was obtained by Erginsoy (19). This expression shows that the relaxation time, and hence the mobility, is dependent on the concentration of neutral impurity in the semiconductor. With this type of scattering process, the mobility is affected by the temperature in a rather indirect manner. At very low temperature, the neutral impurity concentration increases with decrease of temperature causing the mobility to change. However, at still lower temperature, the neutral impurity concentration becomes constant and hence the mobility is independent of the temperature.

2.3 Charge Carrier Concentrations of Semiconductor with Parabolic Band Structure

Under conditions of thermal equilibrium, the energy states which the electrons in a semiconductor acquire are governed by the Fermi-Dirac distribution function. Hence, for a given temperature T,

the probability of finding an electron in a state of energy E_1 in the conduction band is

$$f(E_1) = \frac{1}{1 + \exp[(E_1 - E_F)/k_B T]} \qquad \text{(II-17)}$$

where E_F is the Fermi level and k_B is the Boltzmann's constant. The probability of finding an electron not occupying a state of energy E_2 in the valence band is

$$1 - f(E_2) = \frac{1}{1 + \exp[(E_F - E_2)/k_B T]} \qquad \text{(II-18)}$$

For a semiconductor with a large energy gap, $(E_1 - E_F)$ and $(E_F - E_2)$ are much greater than $k_B T$; and equations (II-17) and (II-18) reduce to

$$f(E_1) = \frac{1}{\exp[(E_1 - E_F)/k_B T]} \qquad \text{(II-19)}$$

and

$$1 - f(E_2) = \frac{1}{\exp[(E_F - E_2)/k_B T]} \qquad \text{(II-20)}$$

The electron and hole concentrations in the conduction and valence bands are respectively

$$n = N_C \exp[(E_F - E_C)/k_B T] \qquad \text{(II-21)}$$

$$p = N_V \exp[(E_V - E_F)/k_B T] \qquad \text{(II-22)}$$

where E_C and E_V are the band edge energies of the conduction and valence bands. N_C and N_V are the effective density of states given as

$$N_c = 2(2\pi m_e^* k_B T/h^2)^{3/2} \qquad \text{(II-23)}$$

$$N_V = 2(2\pi m_h^* k_B T/h^2)^{3/2} \qquad \text{(II-24)}$$

where m_e^* and m_h^* are the density of state effective masses of electrons and holes respectively. If the semiconductor is intrinsic the electron and hole concentrations are equal and the intrinsic carrier concentration n_i is

$$n_i = n_p = p \qquad \text{(II-25)}$$

and for slightly doped semiconductors

$$n_i^2 = np = N_c N_V \exp(-E_g/k_B T) \qquad \text{(II-26)}$$

where $E_g = E_C - E_V$ is the energy gap of the semiconductor.

Consider now the case of an n-type semiconductor containing a donor impurity concentration N_D and an acceptor impurity concentration N_A. Assume that each donor atom and each acceptor atom can furnish one charge carrier. From the condition of electrical neutrality,

$$n = p + (N_D - N_A) - N_D f_D + N_A f_A \qquad \text{(II-27)}$$

where f_D is the probability that the donor atom is not ionized and f_A is the probability that the acceptor atom is not ionized and

$$f_D = \left\{1 + \frac{1}{g_D} \exp[(E_D - E_F)/k_B T]\right\}^{-1} \qquad \text{(II-28)}$$

The [illegible] is given by a similar expression. In the equation [illegible] E_D is the ground state of the donor impurity and the factor g_D is the degeneracy of the ground state, and is usually assumed to be 2. With $n \gg p$, by using equations (II-21) and (II-28), and the fact that $N_D f_D \gg N_A f_A$ equation (II-27) becomes

$$\frac{n\,(n+N_A)}{N_D - N_A - n} = \frac{N_c}{2} \exp\left[-(E_c - E_D)/k_B T\right] \qquad \text{(II-29)}$$

where $(E_c - E_D)$ is the ionization energy of the donors.

At sufficiently high temperatures the intrinsic concentration n_i becomes large compared to $(N_D - N_A)$; equation (II-27) reduces to $n \simeq p$. The semiconductor becomes intrinsic. As the temperature is lowered, the electron concentration becomes a constant,

$$n \simeq N_D - N_A \qquad \text{(II-30)}$$

This is the temperature range of exhaustion where practically no electrons are left in the donor levels. At very low temperatures when $n \ll N_D$, equation (II-29) reduces to

$$n = \frac{N_D - N_A}{N_A} \frac{N_c}{2} \exp\left[-(E_c - E_D)/k_B T\right] \qquad \text{(II-31)}$$

2.4 The Kane Model for Non-parabolic Band Semiconductors

When the energy bands of a semiconductor is not parabolic the equations developed in section 2.3 become invalid and hence a different band model has to be adopted. Kane (20), by means of the $k.p$ perturbation approach, has developed a theory which describes the band structure of indium antinomide in the vicinity of $k=0$. Kane's theory takes into account of the mutual interaction

of three [illegible] bands and one conduction band and lead to the following [illegible] E–k relationships:

$$E_C = \frac{\hbar^2 k^2}{2m} + \frac{E_g}{2} + \frac{1}{2}\left[E_g^2 + \frac{8}{3}P^2 k^2\right]^{1/2} \qquad \text{(II-32)}$$

$$E_{V1} = \frac{\hbar^2 k^2}{2m} \qquad \text{(II-33)}$$

$$E_{V2} = \frac{\hbar^2 k^2}{2m} + \frac{E_g}{2} - \frac{1}{2}\left[E_g^2 + \frac{8}{3}P^2 k^2\right]^{1/2} \qquad \text{(II-34)}$$

$$E_{V3} = -\Delta + \frac{\hbar^2 k^2}{2m} - \frac{k^2 P^2}{3(E_g + \Delta)} \qquad \text{(II-35)}$$

where E_C, E_{V1}, E_{V2} and E_{V3} are the energies in the conduction heavy-hole, light-hole and split-off valence bands respectively; E_g is the principal band gap at $k=0$; P is the Kane's momentum matrix element; Δ is the spin-orbit splitting energy; $\hbar$ is the Planck's constant/2π; m is the electronic rest mass; and the energies are measured from the top of the valence band. Figure II-2 shows the energy band structure of indium antimonide as described by the Kane's theory.

The Kane's model has been developed with the assumption that the crystal lattice is rigid and hence be best approximated by absolute zero temperature data. Ehrenreich (21) points out that, at finite temperatures, the value of E_g is affected by both the lattice dilation and interaction with the phonon field. Since

the interaction with the phonon field produces just a shift [illegible] band [illegible] changing the band curvature [illegible] dilation [illegible] produces a much larger change in band curvature; i.e. in equation (II-32), (II-34) and (II-35) should be replaced by L_g^*, the "effective mass band-gap".

Two properties concerning the band edge effective masses of the conduction and light-hole valence bands can be deduced from equations (II-32) and (II-34). It can be shown that by using the definition of band curvature effective mass

$$m^* = \frac{\hbar^2}{d^2E/dk^2} \qquad \text{(II-36)}$$

and evaluating at $k=0$,

$$m_e^* \simeq m_{lh}^* \simeq \frac{3\hbar^2 E_g^*}{4P^2} \qquad \text{(II-37)}$$

where m_e^* and m_{lh}^* are respectively the band edge effective mass of the conduction and light-hole valence bands. Hence, at $k=0$, m_e^* and m_{lh}^* are equal and are both proportional to E_g^*.

2.5 The Inverted Band Model of Mercury Chalcogenides

The inverted band model was introduced by Groves and Paul (8) to explain the band structure of gray tin. A similar model was later employed by Harman et al (22) in the study of HgTe and HgTe-CdTe alloys. On the basis of the results obtained from thermo-electric power versus hydrostatic pressure measurements Piotrzkowski et al (5) also arrived at the same model. The only difference between the two proposed models is the amount of

ev ... between the conduction and heavy-hole valence bands at $k \neq 0$.

Figure II-3 shows the inverted band model of HgTe. Comparing this with Figure II-2 one can see that the ordering of the Γ_6 and Γ_8 states is inverted. What is usually the light-hole valence band of a normal zincblende structure compound, for example InSb, becomes a conduction band tied by symmetry to the heavy-hole valence band at $k=0$; and what is usually the conduction band becomes a light-hole valence band separated from the heavy-hole valence band at $k=0$. Equations (II-32) and (34) have to be modified to describe the E-k relationship of the conduction and light-hole valence bands. Hence, with reference to Figure II-3,

$$E_c = \frac{\hbar^2 k}{2m} - \frac{|E_g|}{2} + \frac{1}{2}\left[E_g^2 + \frac{8}{3}P^2k^2\right]^{1/2} \qquad \text{(II-38)}$$

$$E_{lh} = \frac{\hbar^2 k^2}{2m} - \frac{|E_g|}{2} - \frac{1}{2}\left[E_g^2 + \frac{8}{3}P^2k^2\right]^{1/2} \qquad \text{(II-39)}$$

There is no actual energy gap in this type of band model. E_g in equation (II-38) and (II-39) represents the energy separation between Γ_6 and Γ_8 states and is defined as

$$E_g = E_{\Gamma_6} - E_{\Gamma_8} \qquad \text{(II-40)}$$

For materials with zincblende structure an overlapping between the conduction and heavy-hole valence band is permissible at $k \neq 0$ in the direction of [111] but the amount is very small, and should be less than 10^{-4} ev theoretically (23).

It has been pointed out by Groves (23) that the usual method of using the "effective mass energy gap" E_g^* in the E-k relationships at finite temperature is not valid for this type of band structure, especially in the case of HgTe. This is supported by the results of recent measurements on lattice dilation (24) and effective mass (25). The work of Piotrzkowski and Porowski (26) has shown that the quantity Q, defined as

$$Q = \frac{|E_g| m}{m^*} \qquad \text{(II-41)}$$

is independent of temperature. Hence equations (II-38), (II-39) and (II-40) are valid at finite temperature for the inverted band structure. With the aid of these equations, it can be shown that the carrier concentration in the conduction band is given by

$$n = \frac{\sqrt{2}}{\pi^2}\left(m_e^* \frac{k_B T}{\hbar^2}\right)^{3/2}\left[\mathcal{F}_{1/2}(\eta) + \beta\left(\frac{5}{2} - 5\xi\right)\mathcal{F}_{3/2}(\eta) + \right.$$
$$\left. + \beta^2\left(\frac{15}{8} + \frac{21}{2}\xi\right)\mathcal{F}_{5/2}(\eta) - 4\xi\beta^3\mathcal{F}_{7/2}(\eta)\right] \qquad \text{(II-42)}$$

$$\beta = \frac{k_B T}{|E_g|}, \quad \xi = \frac{m_e^*}{m}, \quad \eta = \frac{E_F}{k_B T}$$

$\mathcal{F}_j(\eta)$ = Fermi-Dirac Integral

$$= \int_0^\infty \frac{\varepsilon^j \, d\varepsilon}{1 + \exp(\varepsilon - \eta)}$$

and the carrier concentration in the heavy-hole valence band, assumed to be parabolic, is

$$p = \frac{\sqrt{2}}{\pi^2} \left(m_h^* \frac{k_B T}{\hbar^2} \right)^{3/2} \mathcal{F}_{1/2} \left(-\eta - \frac{E_t}{k_B T} \right) \qquad \text{(II-43)}$$

where m_h^* is the density of state effective mass in the heavy-hole band and E_t, the thermal band gap, is defined as

$$E_t = E_c - E_{VI} \qquad \text{(II-44)}$$

at $k \neq 0$.

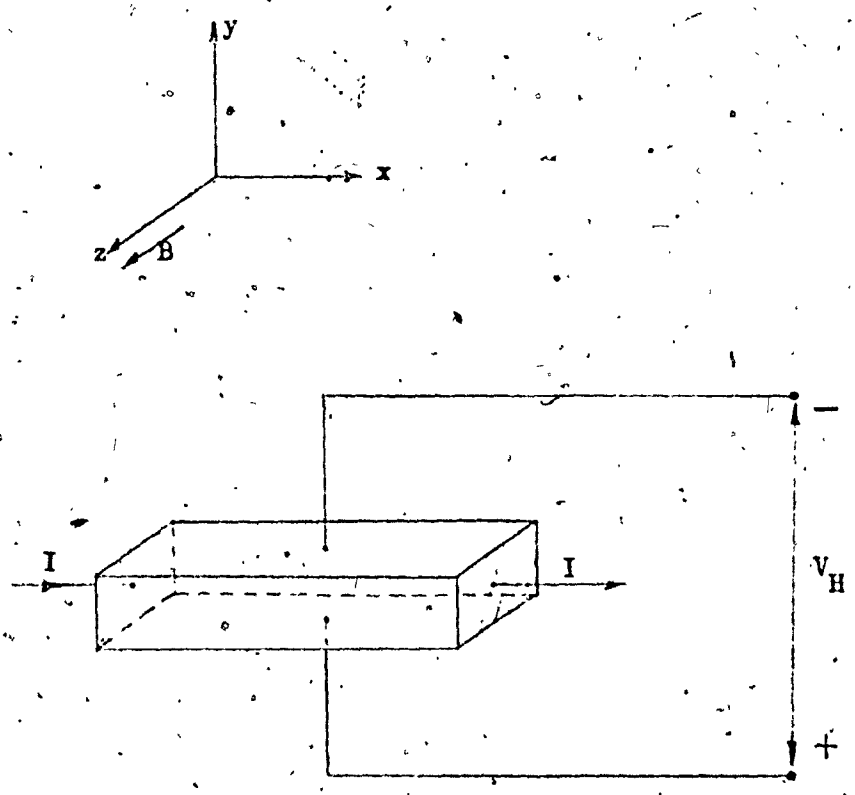

Figure II-1: The Hall Effect Geometry

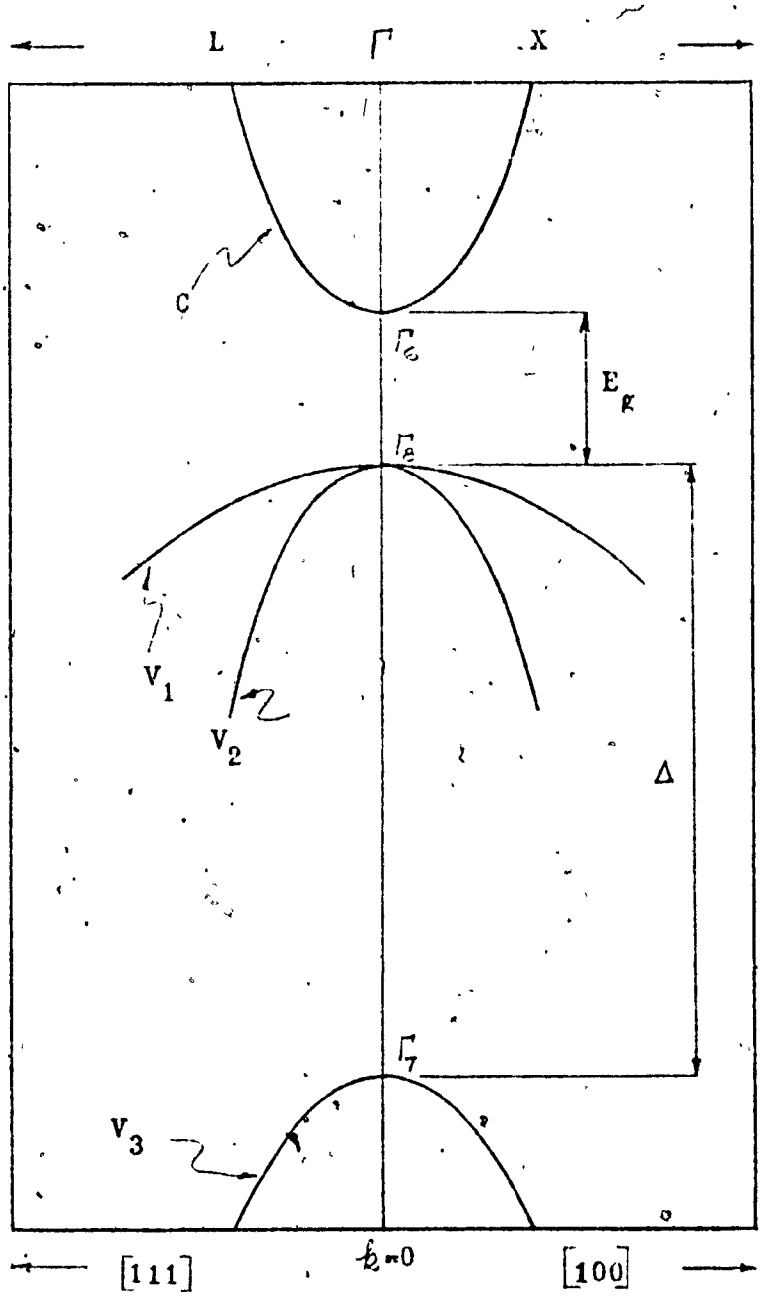

Figure II-2: The Energy Band Diagram of Indium Antimonide InSb

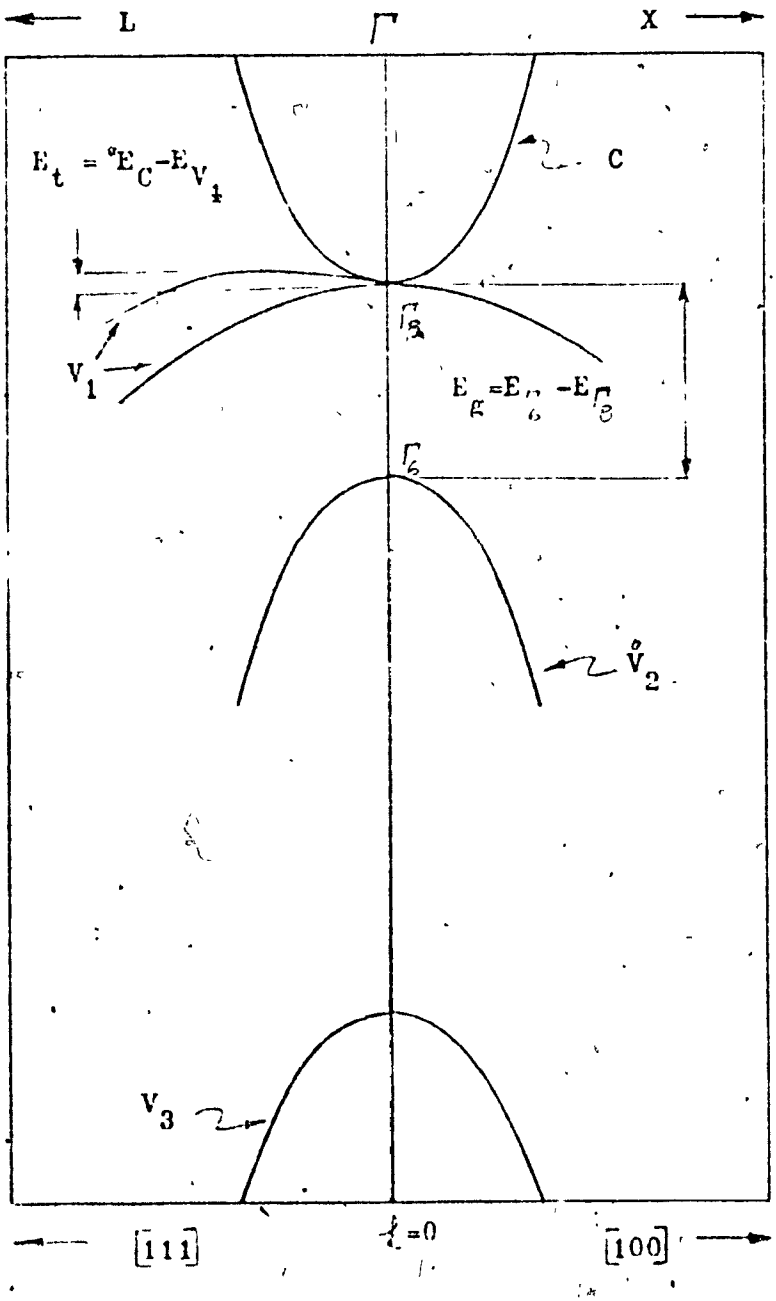

Figure II-3: The Inverted Band Model of Mercury Telluride HgTe

CHAPTER III

EXPERIMENTAL APPARATUS AND TECHNIQUE

3.1 Material Preparation

Mercury telluride crystals were prepared by the modified Bridgman technique using direct synthesis from their semiconductor grade elements, that is, mercury tridistilled and semiconductor grade tellurium from Noranda Company of Canada Ltd. Stoichiometric amounts of mercury and tellurium were positioned into a quartz boat which was then sealed inside a quartz ampeule at 10^{-5} mm Hg pressure. This was then suspended in the horizontal zone refiner using a silicon carbide tube. The hot zone, similar to that described by Harman et al (2), of the zone refiner was set at 675°C and the background furnace at 500°C to insure a mercury vapour pressure of 15 atmospheres inside the ampeule to prevent dissociation. A travelling rate of 0.35 cm/hr was used for synthesis as well as for zone refining the prepared compound. Polycrystals containing large single crystal segments (typical grain size 15x4x4 cm) were obtained typically after 3 zone refining passages. Debye-Scherrer X-ray powder patterns of the synthesized HgTe agreed with published data (27).

Similar conditions were used to grow the mixed crystals. The hot zone temperature was adjusted each time to be approximately

[illegible] the solidus point of the alloys being synthesized. Table III-1 [illegible] stoichiometric [illegible] were used in preparation of the alloys and Figure III-1 shows their approximate melting points.

3.2 Sample Geometry

Contacts used for current and potential leads to connect the Hall sample are generally more highly conducting than the sample itself. Since they have finite size they will distort the potential distribution and hence the Hall voltage measured will be in error. The case which has been most extensively studied is a rectangular parallelpiped with the ends completely covered with highly conducting material to ensure parallel current lines. It is essential that the length to width ratio of the sample to be greater or equal to 4 since a smaller ratio will produce shorting effect of the Hall field. A good discussion of this effect is given by Beer (28). This type of sample has the disadvantage of difficulty in making proper Hall probe alignment and mechanically sound contacts in some materials.

Van der Pauw (29) has derived a method of measuring the Hall coefficient and resistivity of arbitrary shaped samples. This method is advantageous when only small single crystals are available. The restrictions of this method are the sample must be of constant thickness, there must not be cavities in the crystal and small contacts must be made at the periphery of the sample.

Figure III-2 shows the type of sample used in this experiment. The dimensions of the samples were chosen according to the ASTM standard (30). These bridge-shaped samples with integral side arms are often used in place of rectangular parallelpipeds for conventional Hall measurements. The advantages are better alignment of the Hall probes and larger area for making contacts. The current lines will tend to bulge at the side arms and studies (31, 32) of this configuration show error in resistivity of about 2%. However there is no effect on the Hall voltage.

3.3 Sample Preparation

Slices of single crystal of approximately 1 mm thick were cut from the ingots by means of a wire saw specially designed by Dr. E. A. Lorbos for crystal cutting purpose. They were then lapped to a uniform thickness of 0.5 mm with #320 alumina lapping powder. A stainless steel sandblasting mask with exact dimensions of the sample and a slice of the crystal were then placed on the base plate and held in position by means of melting wax over them as shown in Figure III-3. A Hall sample was then cut from the crystal slice by precision sandblasting using the S. S. White model K150 sandblasting unit. A jet pressure of 20 psig was required for efficient cutting and #620 alumina powder was used as the abrasive. Excess undercutting of the sample would occur if the abrasive particles were allowed to be deflected by the base plate and hence a hole was cut on the plate just under where the crystal slice and the mask were positioned. After the sandblasting process

the [illegible] cleaned and degreased by boiling in trichloroethylene, [illegible] and then in methanol.

Contacts to the sample were made by evaporating gold through a mask on the ends and the side arms. This was necessary since reaction of indium solder with HgTe was reported (33). Since all the extremeties of the sample were bevelled, they were completely wrapped around by the gold contacts. Some dimension error was invariably introduced during the sandblasting and evaporation processes, hence the sample was measured with a travelling microscope having an accuracy of ±0.005 mm. The sample was then connected to the sample holder by indium solder using 0.004" diameter silver plated copper wires. The contacts were checked using a curve tracer to ensure ohmic contacts. Figure III-4 shows the assembly of the sample, sample holder and the sample support tube.

3.1 Experimental Apparatus

3.11 The Cryostat

The cryostat used in the Hall effect and electrical resistivity measurements is of type MHD-3L-30N manufactured by Andonian. The schematic drawing of the cryostat is shown in Figure III-5. The sample is mounted at the end of the sample support table beneath the thermometer housing. A resistance heating wire which serves as the sample heater is wound around this housing and is insulated and held in place by means of epoxy. All electrical leads inside the sample chamber are connected to a hermetically sealed connector of

type Bendix PT06A-14-19S (SR). This connector is located at the top end of the sample support tube. The portion of the sample chamber in which the sample is positioned is thermally shielded by a radiation shield. This shield is cooled by the liquid nitrogen in the nitrogen reservoir by thermal conduction. A pressure of less than 10^{-5} mm Hg is maintained in the vacuum chamber by means of an oil diffusion pump to insulate the sample chamber from the outer shell of the cryostat. The temperature in the sample chamber is lowered by admitting liquid helium through a throttle valve and vaporization heater. The exchange gas is extracted from the chamber by means of a high speed rotary pump connected to the off-gas line. Temperatures from 1.5°K to 350°K are obtained by maintaining an exchange gas pressure of 5 mm Hg and by adjusting the power supplied to the sample and vaporization heaters. With the Andonian A-8B manual temperature control system it is possible to maintain temperature to within 0.1°K over the entire temperature range. Two resistance thermometers are used to determine the temperature. The Andonian CG-1AC germanium resistance thermometer is used from 1.5°K to 30°K and the Andonian PR-1 platinum resistance thermometer is used from 30°K to 350°K.

3.42 The Electromagnet

The magnetic field required for the Hall effect measurements is supplied by a 12-inch Varian V-3900 electromagnet with a 3-inch pole gap and a 9-inch pole face. By means of a temperature-controlled Hall effect crystal probe the magnetic field intensity is maintained

to within 1% of the selected value. The field intensity is set by means of a set of dials located in the control panel. A field reversing switch is also provided. The maximum field intensity available is 10 K Gauss.

3.13 The Data Acquisition and Processing System

All the measurements required for this experiment, including the Hall voltages, electrical resistivities, temperatures and magnetic field intensities, were recorded and processed with the aid of a computer system. This data acquisition and processing system was originally designed by Dr. A. Kipling of the Physics Department at Sir George Williams University to initiate a research program on electrical properties of various semiconductor materials. A block diagram of the system is shown in Figure III-6. The heart of this system is the Digital Equipment Corporation PDP-8/I general purpose digital computer. This is a single address, parallel machine with fixed word length (12 bits) and a basic 4 K random accessable core memory.

Information interchange between the operator and the computer is accomplished either through the operator console or the teletype unit. The teletype ASR33 has the input facility of a keyboard and a paper-tape reader and the output facility of a printer and a paper-tape punch. This machine operates with serial 8-level ASCII code characters at a rate of 10 characters per second.

Experimental measurements in the form of electrical voltages are input to the computer through a guarded relay multiplexer

[illegible] digital voltmeter. The multiplexer, controlled by [illegible], a Digital Equipment Corporation type AD11 [illegible]. Each of their modules can handle two analog signals simultaneously and hence a maximum of 16 analog signals can be multiplexed to the computer through the digital voltmeter. The digital voltmeter is a Hewlett-Packard Model 2402A integrating digital voltmeter which has a maximum measuring rate of 13 measurement per second. The input impedance is 10^9 ohms and the accuracy is 0.01% of the voltage reading. Five voltage range are provided; from 0.1 to 1000 volts in steps of 10^1 times. Aside from a visual display by a six-digit nixie assembly the measured voltage is also output in the form of binary-coded-decimal through a connector at the back of the instrument.

The on-line plotting of processed data facility is provided through the service of a Houston Model DP-I-1 digital plotter which has a maximum drawing rate of 3 inches per second and a resolution of 0.01 inch per step. The unprocessed data is recorded by a Peripheral Equipment Corporation Model 3 20-7 digital magnetic tape unit for off-line processing. The unit has 7 tracks and operates at a read/write speed of 25 inches per second. The storage density of the unit is 556 bytes per inch.

The two computer program packages used to record and process the experimental measurements are modified versions of the ones originally developed by R. Krawczynuik. A complete listing and detailed description of their usage and requirement can be found in (34). The main features of the on-line program package are :

a) real-time acquisition of data voltages from electrical resistivity and Hall effect measurements; b) printing of the data voltages on the teletype; c) storage of this data on magnetic tape; and d) on-line plotting of the Hall coefficient as a function of the reciprocal temperature. The second program package enables the off-line plotting of either the logarithm of the electrical resistivity as a function of the reciprocal temperature and/or the logarithm of the Hall mobility as a function of the logarithm of the temperature. The modifications made on the on-line program package are to eliminate the associated thermomagnetic and galvonomagnetic effects which are present during the measurement of Hall voltage as a function of temperature. A description of these effects and the procedure required to eliminate them are given in section 3.5.

3.44 Measurement Technique

Figure III-7 shows the schematic drawing of the electrical wiring between the Hall sample, the cryostat, the various power supplies and the data acquisition system. The Hall sample current is supplied by a constant current source, Hewlett-Packard Model 6207B. The direction of the sample current can be reversed by means of the two-position make-before-break rotary switch. The magnitude of this current is input to the computer in the form of a voltage-drop across a 100K ohm standard resistor which is connected in series with the constant current source. The magnetic field intensity is determined by a calibration curve that is stored in the computer. The calibration curve relates the field intensity,

measured by [illegible] Model 822 rotating coil gaussmeter, as a function of the voltage-drop across a 0.33 ohm standard resistor connected in series with the field winding of the electromagnet. A similar technique is used to determine the temperature. By means of the voltage-drop across the 10K ohm standard resistor and the germanium and platinum thermometers, the resistance of the thermometers are calculated. The temperature is then obtained by referring to the calibration curves which give the temperature as a function of the thermometer resistances.

3.5 A Procedure to Eliminate Certain Associated Effects in Hall Voltage Measurements

In order to obtain accurate Hall voltage measurement certain associated effects which give rise to voltage drops at the Hall probes must be eliminated. A parallelpiped sample shape is chosen to describe these effects. As the physical size of the Hall sample is usually very small (1×0.1×0.05 cm typical size) it is extremely difficult to align the Hall probes properly. Invariably, some misalignment is bound to occur. Figure III-8(a) shows the equipotential lines along the sample when it is subjected to a current at its ends. Because of the misalignment the Hall probes, A and D are at different potentials. This potential drop across the probes is known as the "IR drop". It is dependent on the direction of the current but is independent of the magnetic field.

The electrons which constitute the sample current do not move across the sample with the same velocity. The faster electrons

will follow a different path when a magnetic field with intensity B is applied perpendicular to the sample than the slower electrons. Hence more energy will be transported to one side of the sample than the other, resulting in a temperature difference, T_A-T_D, as shown in Figure III-8(b). This effect is known as the Ettingshausen effect. Since the Hall probes and the sample are of different materials, they form a thermocouple and thus generating a potential across the sample.

When the two ends of the Hall sample are subjected to a temperature difference a thermal current will flow across the sample as shown in Figure III-8(c) and (d). In the Nernst effect, a potential, V_N, will appear across the sample when a magnetic field is applied perpendicular to the sample. Under these same conditions a temperature difference across the sample is also produced. This is known as the Righi-Leduc effect.

Because of all these effects the voltage measured across the Hall probe is a sum of V_H, the Hall voltage; V_{IR}, the voltage due to probes misalignment; V_E, the voltage due to the Ettingshausen effect; V_N, the voltage due to Nernst effect; and V_{RL}, the voltage due to Righi-Leduc effect. All these voltages, with the exception of V_E, can be eliminated by taking a series of measurements with all possible combinations of current, I, and magnetic field, B, directions. Noting that V_H and V_E are dependent on both I and B, V_N and V_{RL} are dependent only on B and V_{IR} is dependent only on I, the measurements will give, for

$$(+B, +I): \quad V_1 = V_H + V_E + V_N + V_{RL} + V_{IR} \qquad \text{(III-1)}$$

$$(+B, -I): \quad V_2 = -V_H - V_E + V_N + V_{RL} - V_{IR} \qquad \text{(III-2)}$$

$$(-B, -I): \quad V_3 = V_H + V_E - V_N - V_{RL} - V_{IR} \qquad \text{(III-3)}$$

$$(-B, +I): \quad V_4 = -V_H - V_E - V_N - V_{RL} + V_{IR} \qquad \text{(III-4)}$$

Hence

$$\frac{V_1 - V_2 + V_3 - V_4}{4} = V_H + V_E \qquad \text{(III-5)}$$

The Ettingshausen effect can be minimized by immersing the Hall sample in a high thermal conductivity medium. Under this condition V_E is usually very small and is generally neglected. Some relative magnitudes of these effects are given by Smith (35).

3.6 Experimental Procedure

The on-line computer program package was loaded and stored in the computer and the cryostat was filled with liquid helium. The sample dimensions were then entered to the computer through the teletype. To ensure that the magnetic field was perpendicular to the sample, the magnet was rotated about its vertical axis and was locked in position where the Hall voltage was maximum. Liquid helium was then emitted to the sample chamber and the sample was allowed to be cooled down to 1.5°K by adjusting the power supplied to the vaporization heater while maintaining the chamber pressure at 5 mm Hg. The resistivity measurement were taken with the magnetic field off and the Hall measurements were taken according to equation (III-1) to (III-5). A sample current of 80 mA was used for all

samples. A magnetic field intensity of 8 KG was used for HgTe and 1 KG for all other samples. Measurements were taken from 1.5°K to 350°K in all cases.

TABLE III-1

STOICHIOMETRIC COMPOSITION OF $HgTe_xSe_{1-x}$ ALLOYS USED IN CRYSTAL PREPARATION

Compound (At. Fraction)	Hg (gm)	Te (gm)	Se (gm)
HgTe	60.4182	38.4361	———
$HgTe_{.8}Se_{.2}$	56.6275	28.8165	4.4577
$HgTe_{.6}Se_{.4}$	60.2862	23.0088	9.4915
$HgTe_{.4}Se_{.6}$	60.6523	15.4323	14.3254
$HgTe_{.2}Se_{.8}$	61.9648	7.8831	19.5138
HgTe	56.4860	———	22.2229

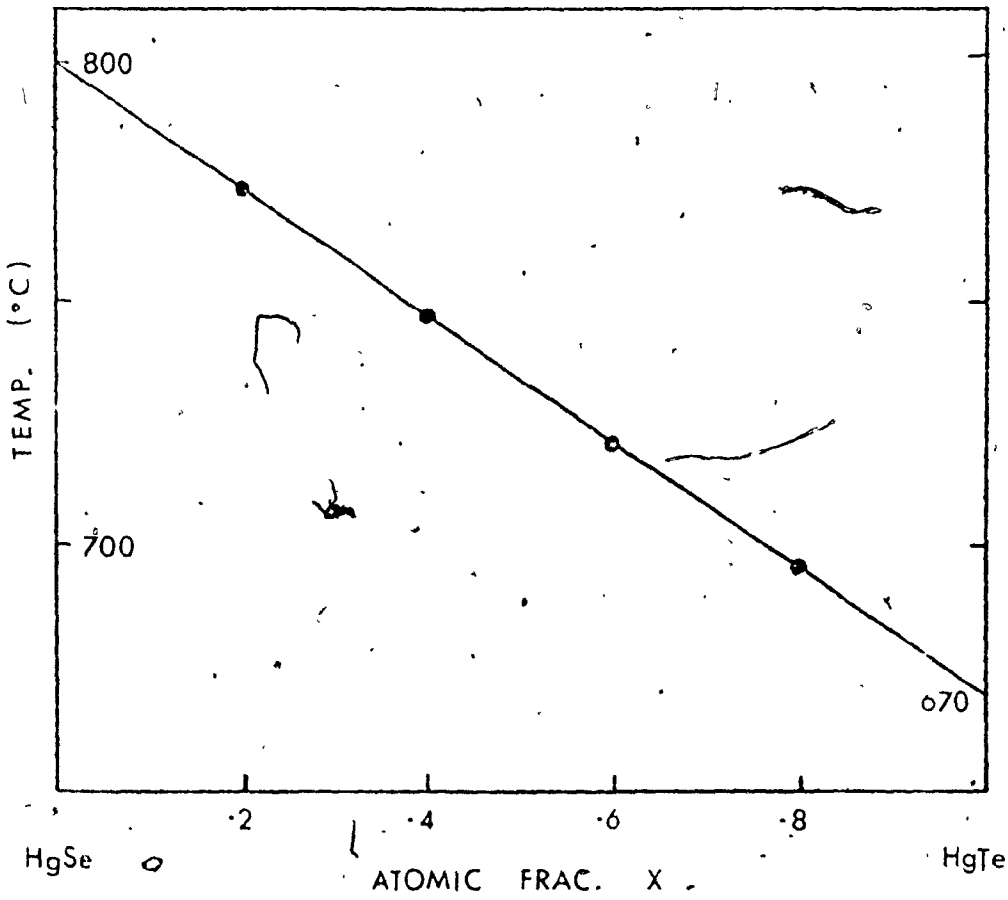

Figure III-1: Melting Points of Mercury Chalcogenides $HgTe_xSe_{1-x}$

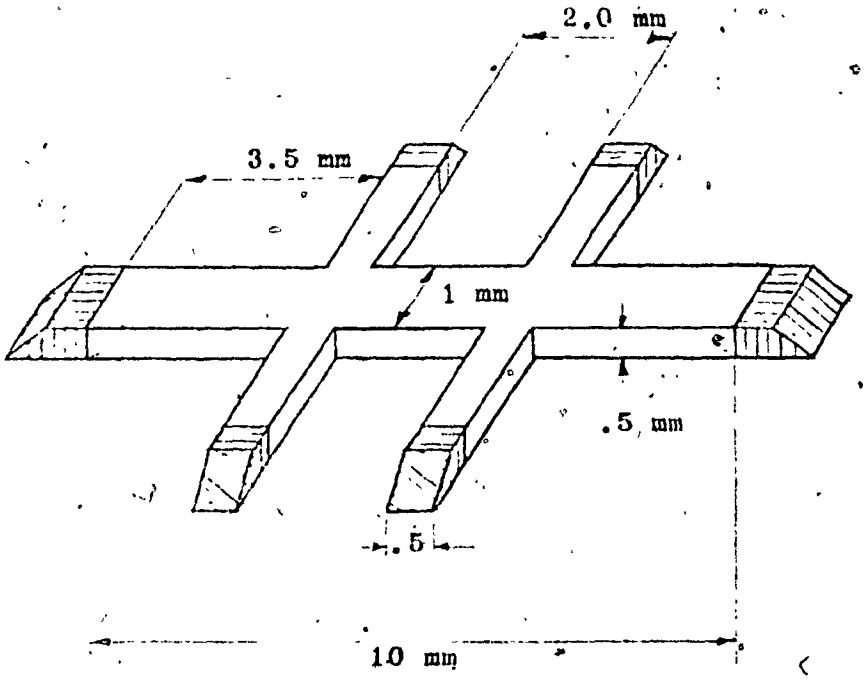

Figure III-2: Hall Effect Bridge-Shaped Sample Showing Evaporated Gold Contacts (Shaded Area)

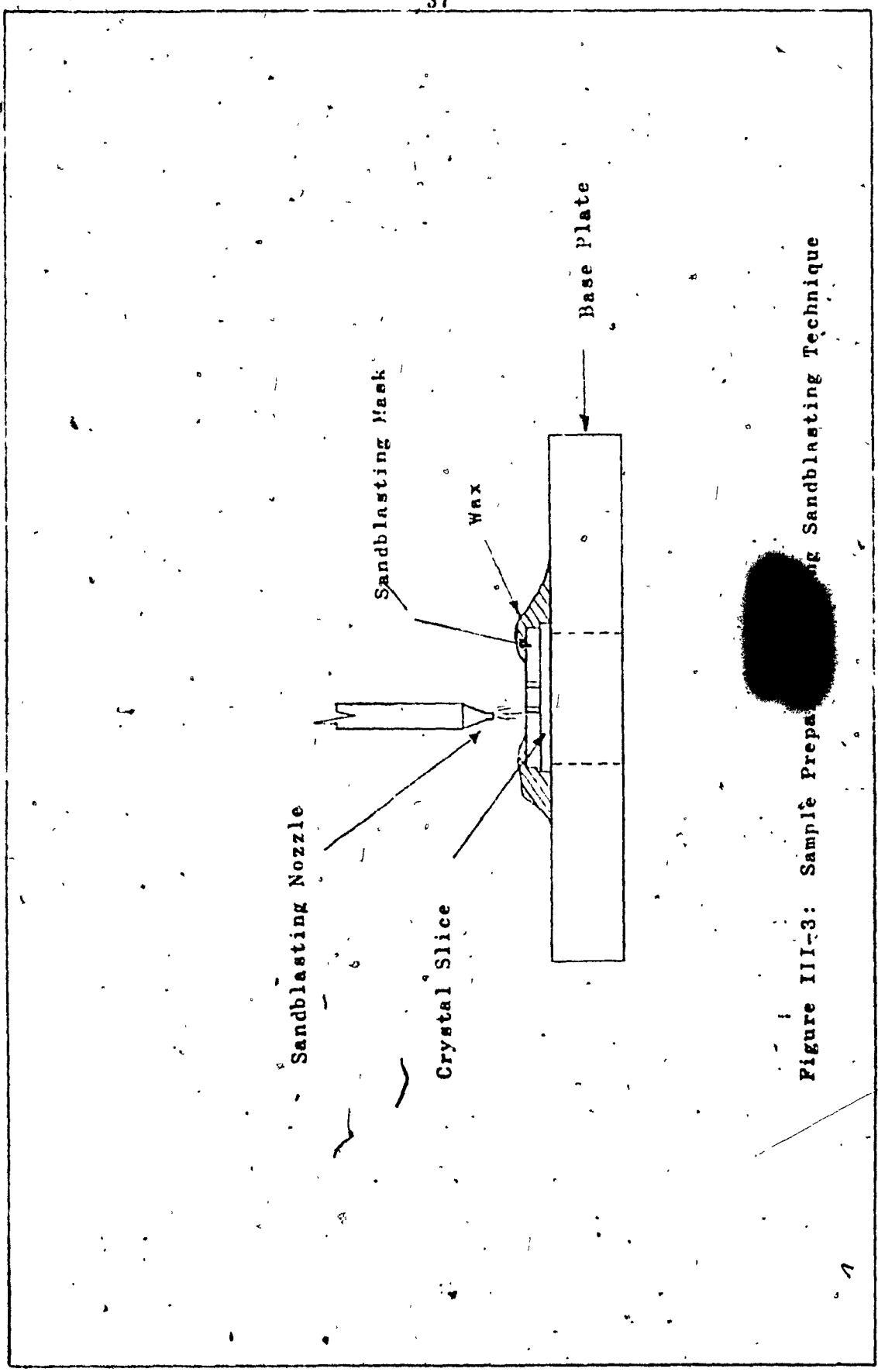

Figure III-3: Sample Prepa[illegible] Sandblasting Technique

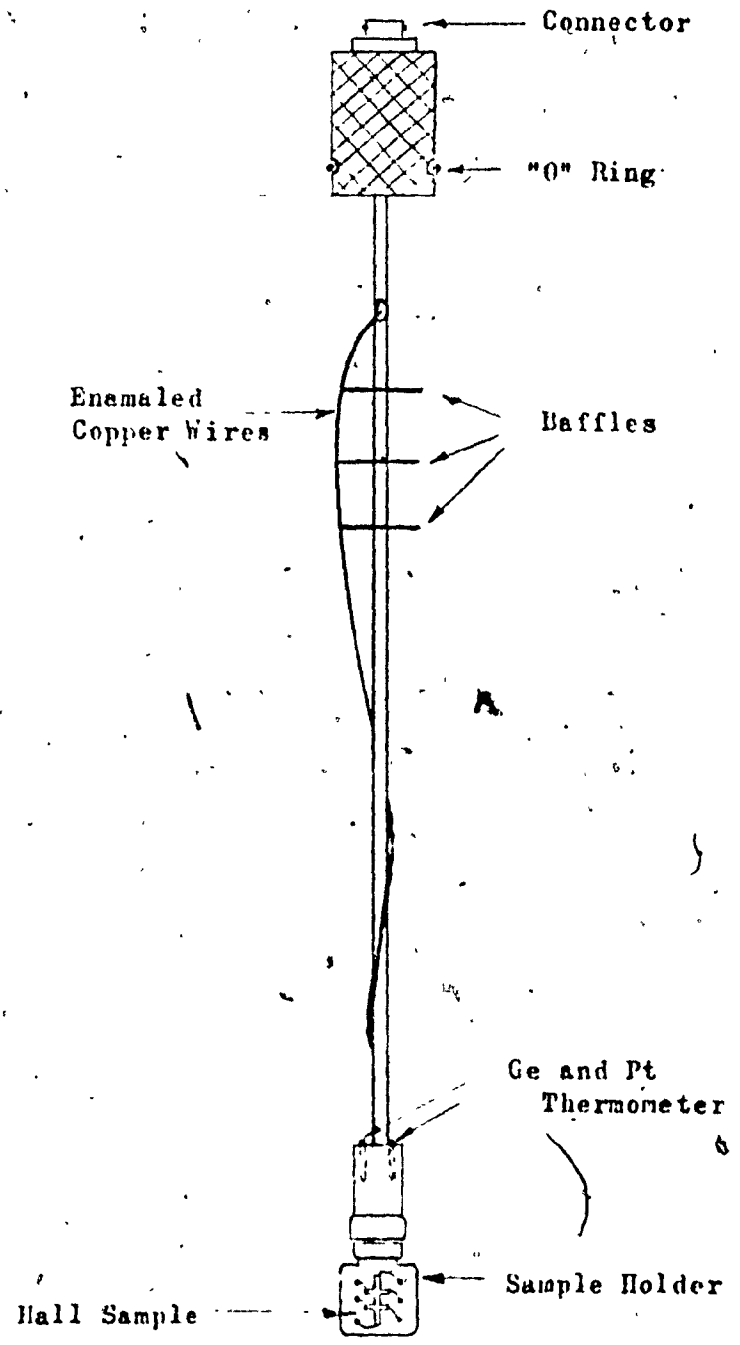

Figure III-4: Sample Support Tube Assembly Shown with Sample Mounted

LEGEND

A Electrical Connectors
B Off-Gas Line
C Helium Fill and Vent
D Insulation Line
E Nitrogen Vent
F Outer Shell
G Nitrogen Reservoir
H Helium Well
I Insulation Space
J Outer Tail Section
K Nitrogen Temperature Radiation Shield
L Sample Heater
M Vaporization Heater
N Exchange Gas Chamber
O Capillary
P Throttle Valve
Q Sample Support Tube
R Throttle-Valve Stem
S Nitrogen Fill
T Helium Gauge Port
U Throttle-Valve Top Works

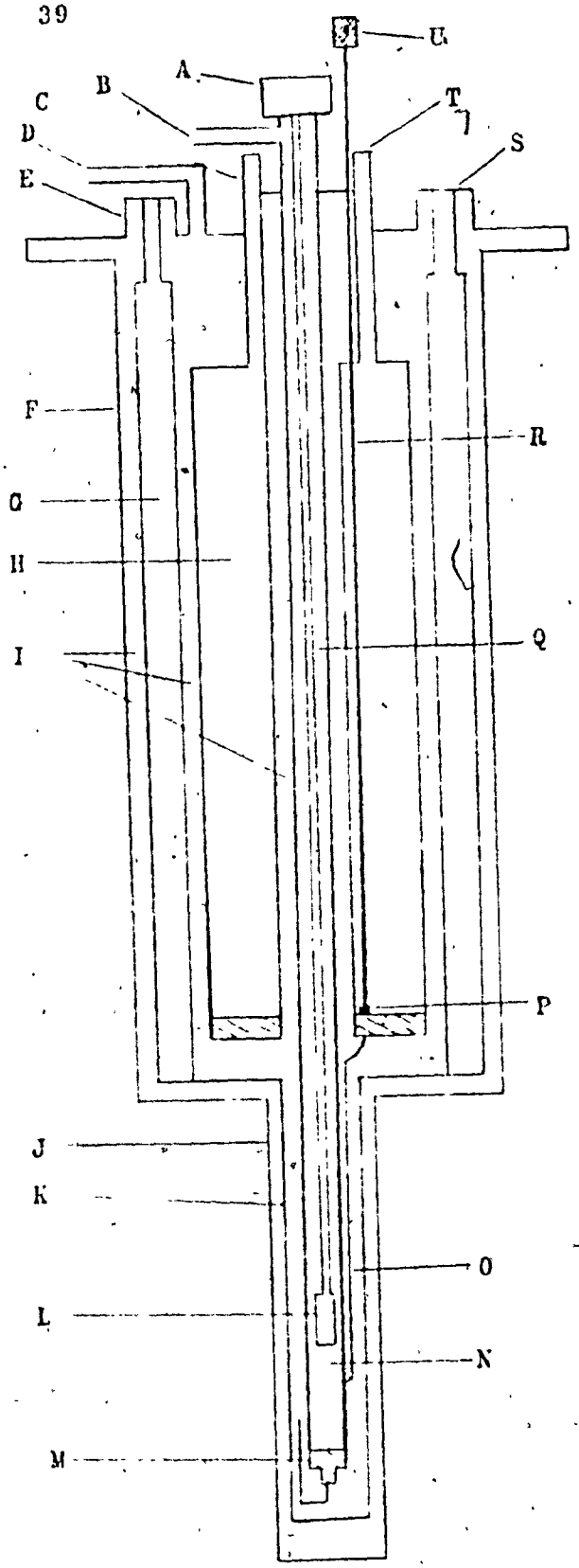

Figure III-5: Schematic Drawing of the Low-Temperature Cryostat (After Krawczyniuk)

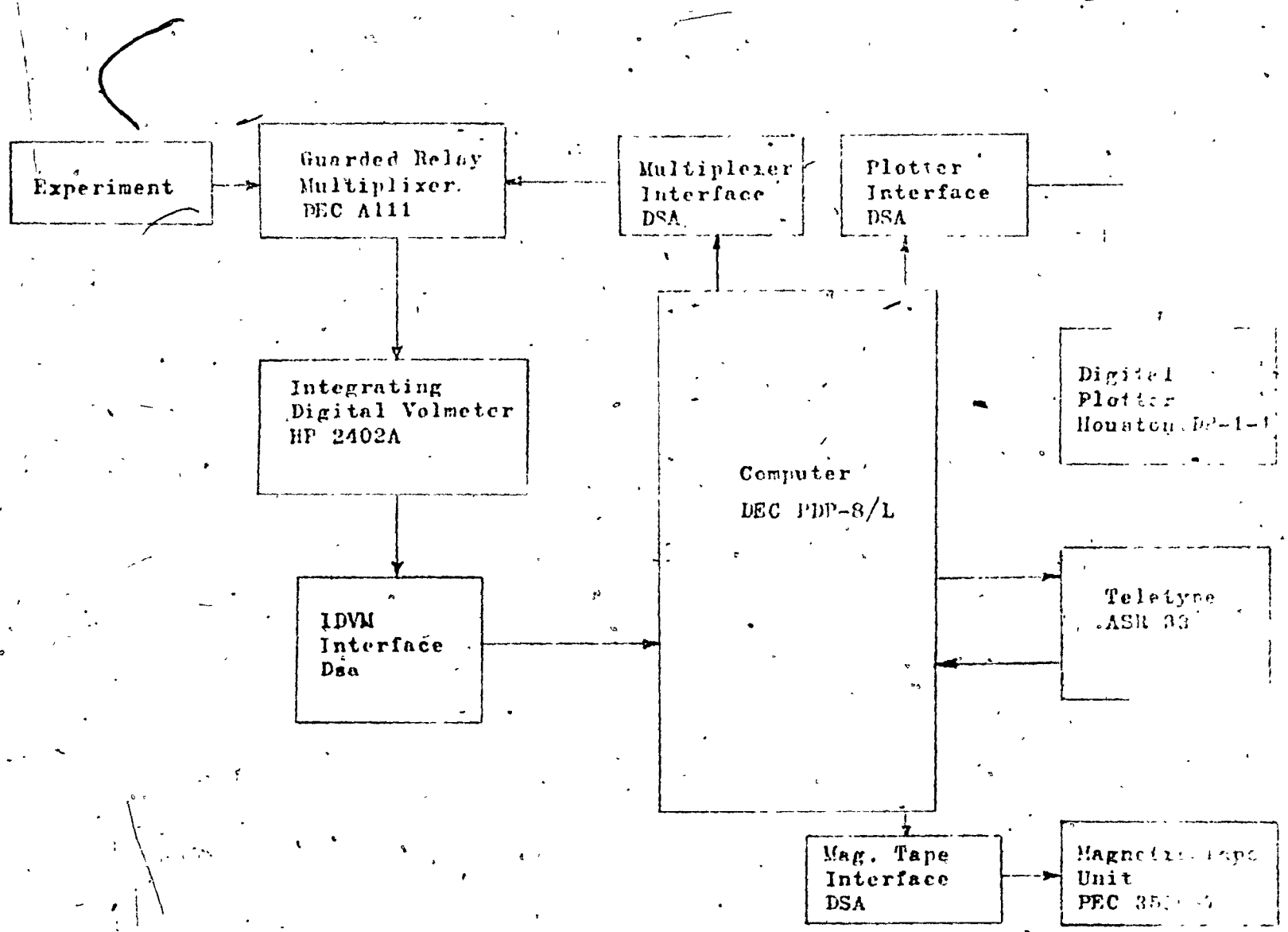

Figure III-6: Block Diagram of the Data Acquisition and Processing Stetem

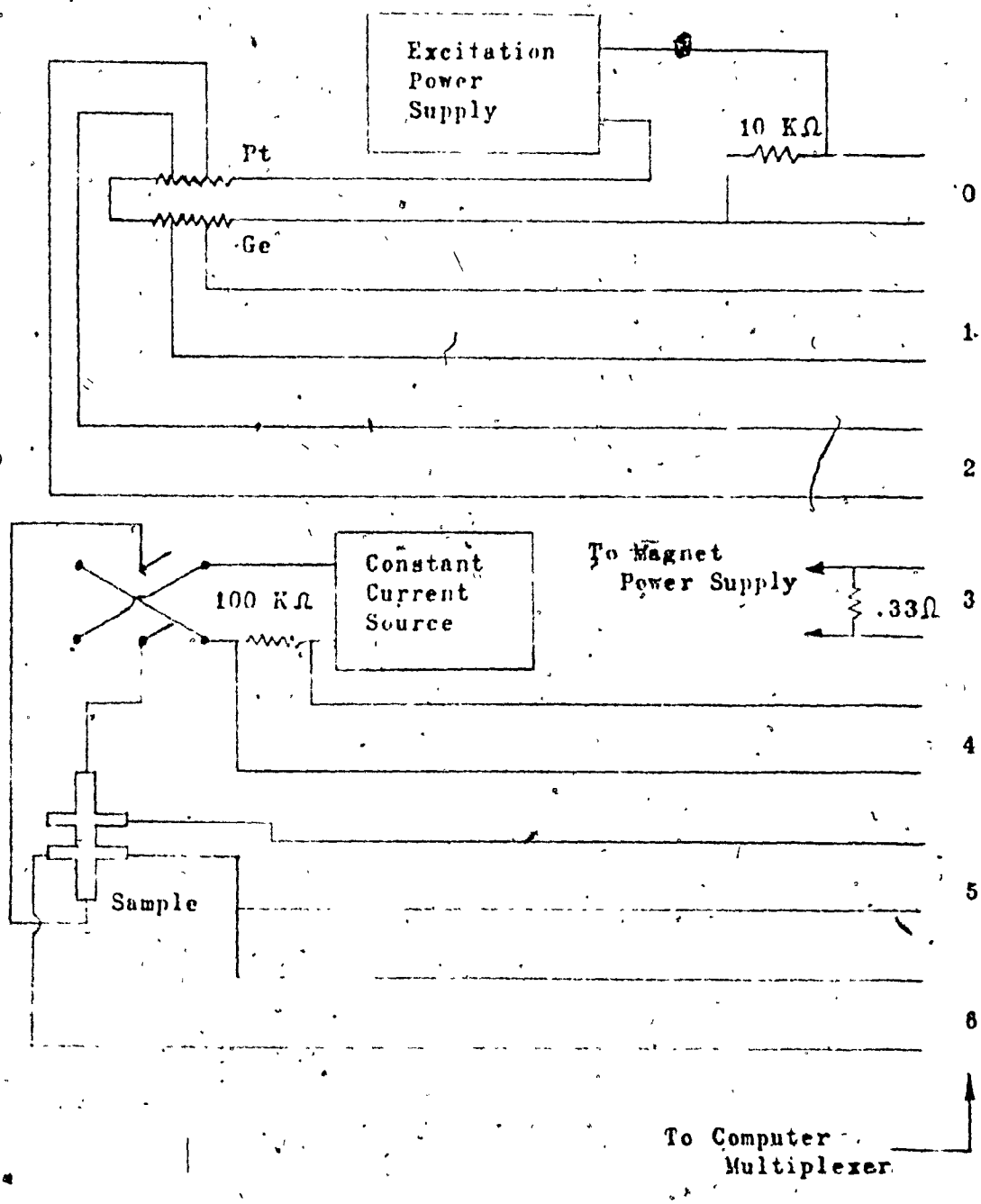

Figure III-7: Wiring Diagram of the Low Temperature Hall Effect Measurement System

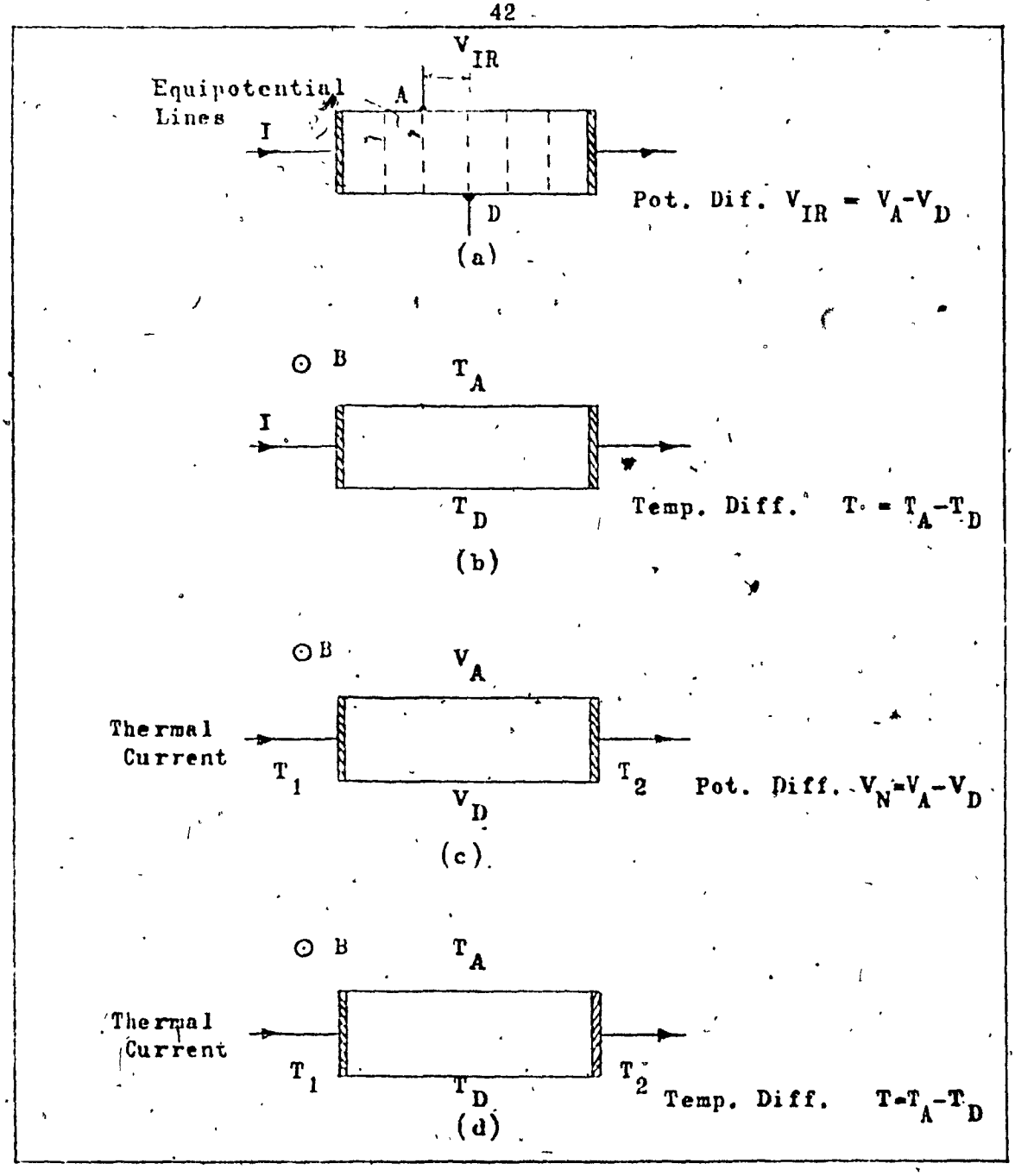

Figure III-8: Associated Effects Present in Hall Voltage Measurement (a) Potential Drop Due to Hall Probes Misalignment (b) Ettingshausen Effect (c) Nernst Effect (d) Righi-Leduc Effect

CHAPTER IV

INTERPRETATION OF RESULTS

4.1 Experimental Results

Hall effect and electrical resistivity measurements were performed on mercury telluride, selenide and their alloys ($HgTe_xSe_{1-x}$, $\Delta x = 0.2$) from 1.5°K to 350°K. A sample current of 80 mA and a magnetic field intensity of 1K Gauss were used for all samples with the exception of HgTe. The Hall voltage on the HgTe sample was found to be very small with 1K Gauss magnetic field and a field strength of 8K Gauss was required to obtain repeatable results. Erratic measurements were obtained for $HgTe_{.2}Se_{.8}$. It was found later that there were hairline fractures on the sample and hence the experimental data on this sample were discarded.

Information obtained from these measurements is given in the following paragraphs in the form of Hall coefficients, electrical resistivity and Hall mobility. Table IV-1 gives their values for all the materials studied at 295°K, 77°K and 1.5°K.

4.11 Hall Coefficient

Figure IV-1 shows the temperature dependence of the Hall coefficient of HgTe. The shape of the curve is typical to a p-type semiconductor with the Hall zero occuring at 53.4°K. The positive

R_H branch rises sharply from the Hall zero temperature but flattens out quickly as the temperature decreases. The negative R_H branch decreases (absolute value of R_H increases) as the temperature increases passing through a minimum at 189°K before reaching the intrinsic region. From the shape of this Hall coefficient curves a few facts can be deduced: (a) the material is p-type; (b) the fact that the exhaustion region (flat portion of positive R_H branch) extends down to 1.5°K indicates that the ionization energy of the impurities present in the semiconductor is extremely low; (c) the low value of R_H in the exhaustion region means that the impurity concentration of the material is very high; (d) this high impurity concentration combined with the occurrence of the Hall zero at low temperature (53.4°K) indicates that the energy gap of HgTe is very small; (e) the sharp p- to n-type transition plus a large ratio of $\left|R_{H_{min}}\right| : \left|R_{H_{exh}}\right|$ implies that the mobility ratio has a large value.

The Hall coefficient curves for mercury selenide and the alloys are shown in Figure IV-2. With the exception of mercury selenide, all the alloys give typical n-type Hall coefficient curves decreasing monotonically from exhaustion to intrinsic regions. In all cases the curves exhibit wide exhaustion regions extending down to 1.5°K and hence indicating extremely low ionization energies of impurities. The Hall coefficient of the HgSe sample is independent of temperature from 1.5°K to 350°K. This is mainly due to the extremely high impurity concentration which masks out the characteristics of the R_H curve in the temperature range where all measurements were taken.

4.12 Electrical Resistivity

The electrical resistivity as a function of temperature for the mercury chalcogenides is given in Figure IV-3. The curves show that the resistivities of these materials are independent of temperature in the lower temperature range (from about 1.5°K to 50°K). This means that the conduction processes in these materials are dominated by ionized impurities in the low temperature range. In the higher temperature region (from about 50°K to 350°K) the resistivities of HgTe, $HgTe_{.8}Se_{.2}$ and $HgTe_{.6}Se_{.4}$ decrease as the temperature increases. This negative temperature coefficient of resistivity is typical of semiconductor as it enters into the intrinsic range. It is interesting to note that as the amount of selenium increases in the alloy composition the temperature coefficient of the resistivity becomes less and less negative; and for $HgTe_{.4}Se_{.6}$ the coefficient is positive. The positive temperature coefficient of the resistivity of HgSe could be due to the high impurity concentration of the sample and the high temperature dependence of the electron mobility. Rodot et al (36) found that around room temperature the Hall mobility is proportional to T^{-2} and Gobrecht et al (37) reported a $T^{-3.5}$ dependence between 300°K and 500°K.

4.13 Hall Mobility

Figure IV-4 shows the variation of Hall mobilities of the mercury chalcogenides with temperature. In the higher temperature region all the mobility curves tend to the same slope of -1.5.

This is typical of lattice scattering by acoustic phonons. However, this temperature dependence is much smaller than those reported by Redei et al (36) and Gobrecht et al (37). Moreover, this $T^{-1.5}$ dependence of mobility is too small to account for the positive temperature coefficient of HgSe and $HgTe_{.4}Se_{.6}$. For HgTe, the acoustic scattering region start from about $300^{0}K$ and for all the alloys and HgSe the region start from about $50^{0}K$. With the exception of HgTe, the mobility curves are flat at lower temperature region indicating that neutral impurities rather that ionized impurities scattering is predominant.

4.2 Analysis of Results

4.21 The Conventional Two-Carrier Model

The model adopted for this analysis consists of one conduction band and one valence band and both are parabolic. Experimental Hall coefficient data of HgTe are used to determine the validity of this model.

The impurity concentration of a p-type semiconductor can be obtained experimentally from the fact that in the exhaustion region

$$p \simeq N_A - N_D \qquad \text{(IV-1)}$$

and since this is the only type of carrier present of this temperature

$$R_{Hexh} = \frac{1}{e(N_A - N_D)}$$

$$(N_A - N_D) \simeq \frac{1}{R_{H_{exh}} e} \qquad \text{(IV-2)}$$

where $R_{H_{exh}}$ is the Hall coefficient in the exhaustion region. At all temperatures, the electrical neutrality condition holds, that is,

$$\therefore p \simeq (N_A - N_D) + n \qquad \text{(IV-3)}$$

Now, equations (II-5) and (II-26) are given as

$$R_H = -\frac{r}{e} \cdot \frac{b^2 n - p}{(bn + p)^2}$$

$$n_i^2 = np = N_C N_V \exp(-E_g/k_B T)$$

Hence, if r and b are known, n_i for different temperatures can be obtained by solving equations (II-5), (II-26), (IV-2) and (IV-3). A plot of $\ln(n_i/T^{1.5})$ versus $\ln(1000/T)$ would give a straight line with a slope equal to $-E_g/2000k_B$.

The value of the scattering factor r ranges from 1 to 2 depending on the scattering processes. A value of unity is usually adopted if the scattering process of the material is not known. The criteria for the determination of r is discussed by Putley (38). In this anslysis r is taken to be unity.

The mobility ratio b is usually assumed to be independent on temperature and is given as (38)

$$\frac{|R_{H_{min}}|}{|R_{H_{exh}}|} = \frac{(b-1)^2}{4b} \qquad \text{(IV-4)}$$

[illegible] Hall coefficient at the minimum of the negative Hall [illegible]

Figure IV-5 shows the plot of $\ln\left[n_i/T^{1.5}\right]$ versus $1000/T$. The graph is not linear as is predicted by theory. From about 170°K downwards the quantity $n_i/T^{1.5}$ becomes independent of temperature. Such a behaviour cannot be accounted for even by taking into consideration of temperature dependence of E_g and b. Hence, it is concluded that HgTe does not have the band structure as prescribed by this simple two-carrier model.

4.22 The Inverted Two-Carrier Model

The model used in this analysis is described in section 2.5. Only the conduction and heavy-hole valence bands are taken into account. The object of the analysis is to fit the experimental Hall coefficient curve of HgTe using this theoretical model.

The theoretical electron and hole concentrations at a particular temperature are generated using equations (II-42) and (II-43) and by adjusting η until equation (IV-3) is satisfied. The theoretical Hall coefficient curve is obtained by substituting the generated n's and p's into equation (II-5).

The variation of mobility ratio with temperature is taken into account by assumming b to vary linearly with temperature. Equation (IV-4) gives the value of b at the temperature where the Hall minimum occurs. The value of b at the Hall zero is determined from the relationship that at this temperature

$$b^2 n = p \qquad \text{(IV-5)}$$

The mobility ratio for the HgTe sample obtained is

$$b(T) = 20 + .06T \qquad \text{(IV-6)}$$

Table IV-2 gives the values of the parameters required for the analysis.

A series of Hall coefficient curves were generated by adjusting the value of the thermal energy gap E_t. The two curves which give the best fit to the experimental data are obtained when E_t=0 and -0.001 ev respectively. Both of these curves are shown in Figure IV-1. From about 130°K the theoretical curves start to deviate from the experimental results. There are two possible causes for this deviation. The first possible cause is due to the simple temperature dependence of the mobility ratio assumed in the analysis. A normalized mobility ratio curve is shown in Figure IV-6. The curve is obtained by substituting the theoretical carrier concentrations and the experimental R_H into equation (II-5) and solve for b. It is evident that the temperature dependence of the mobility ratio used in the analysis is oversimplified. Basing on the shape of the normalized curve a more refined b(T) can be derived. However, further study on the scattering mechanism in HgTe is required to justify this.

The second possible cause is that the two-carrier model is inadequate at higher temperatures. E_g is very temperature sensitive and decreases rapidly as thetempefature rises so that the deep lying light holes cannot be neglected anymore.

The curve fitting process in this analysis is very tedious and a computer program has been written for this purpose. The

listing of the program is found in the appendix.

The same technique was used to analyse the experimental data of all the alloys. The values of the band parameters required for the analysis were assumed to vary between those of HgTe and HgSe. Results obtained are inconclusive since the value of E_t which gives the best curve fit of the alloy oscillates between $\pm.01$ ev instead of varying smoothly as the alloy composition.

TABLE IV-1

HALL COEFFICIENT, HALL MOBILITY, ELECTRICAL RESISTIVITY AND IMPURITY CONCENTRATION OF THE MERCURY CHALCOGENIDE CRYSTALS

Compound	Type	Impurity Conc. (cm^{-3})	Temp. (^{o}K)	Hall Coeff. (cm^3/coul.)	Elec. Rec. (ohm-cm)	Hall Mob. (cm^2/v.s.)
HgTe	p	1.17×10^{18}	1.5	5.27	2.50×10^{-2}	2.07×10^{2}
			77	- 10.36	2.10×10^{-2}	4.98×10^{2}
			295	- 26.49	1.80×10^{-3}	1.44×10^{4}
$HgTe_{.8}Se_{.2}$	n	1.09×10^{16}	1.5	-573	6.81×10^{-3}	9.49×10^{4}
			77	-335	2.81×10^{-3}	1.19×10^{5}
			295	- 14.21	6.09×10^{-4}	2.33×10^{4}
$HgTe_{.6}Se_{.4}$	n	2.25×10^{17}	1.5	- 27.90	6.78×10^{-4}	4.10×10^{4}
			77	- 27.83	6.51×10^{-4}	4.26×10^{4}
			295	- 7.15	5.11×10^{-4}	1.40×10^{4}
$HgTe_{.4}Se_{.6}$	n	4.31×10^{17}	1.5	- 14.52	3.15×10^{-4}	4.61×10^{4}
			77	- 14.53	3.19×10^{-4}	4.53×10^{4}
			295	- 7.67	4.50×10^{-4}	1.71×10^{4}
HgSe	n	3.13×10^{18}	1.5	- 2.06	5.88×10^{-5}	3.51×10^{4}
			77	- 2.06	5.63×10^{-5}	3.66×10^{4}
			295	- 1.95	1.55×10^{-4}	1.26×10^{4}

TABLE IV-2

VALUES OF PARAMETERS USED FOR ANALYSIS OF HgTe HALL COEFFICIENT

		Ref.
Kane's momentum matrix element	$P = 8.3\times10^{-8}$ ev cm	(10)
Energy gap	$E_g = -0.3$ ev at $4.2^{\circ}K$	(9)
	$= -0.15$ ev at $295^{\circ}K$	(4,39)
Density of state effective mass	$m_h^* = 0.55m$	(39)
Mobility ratio	$b(T) = 20 + .06T$	

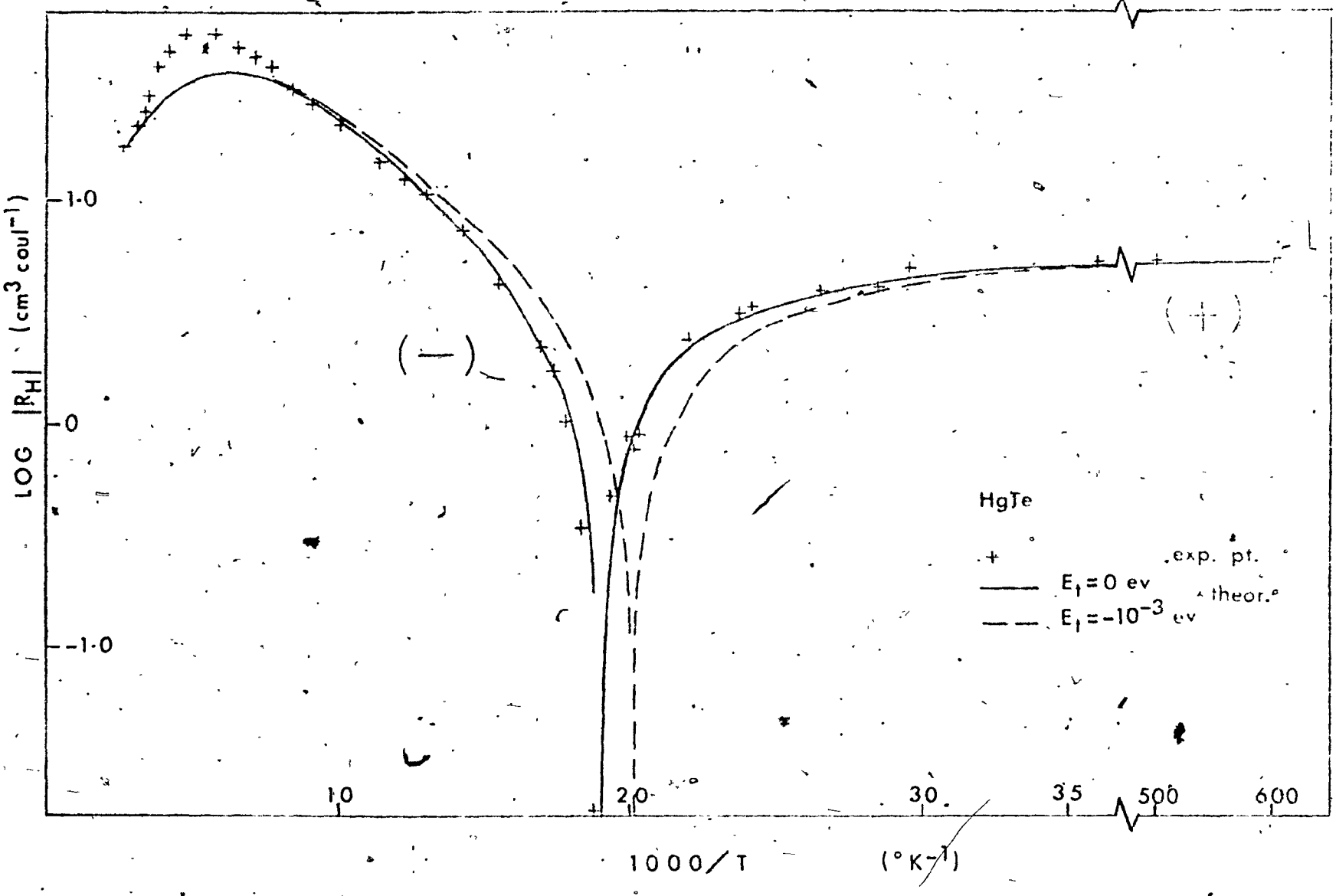

Figure IV-1: Hall Coefficient of HgTe as a Function of Temperature

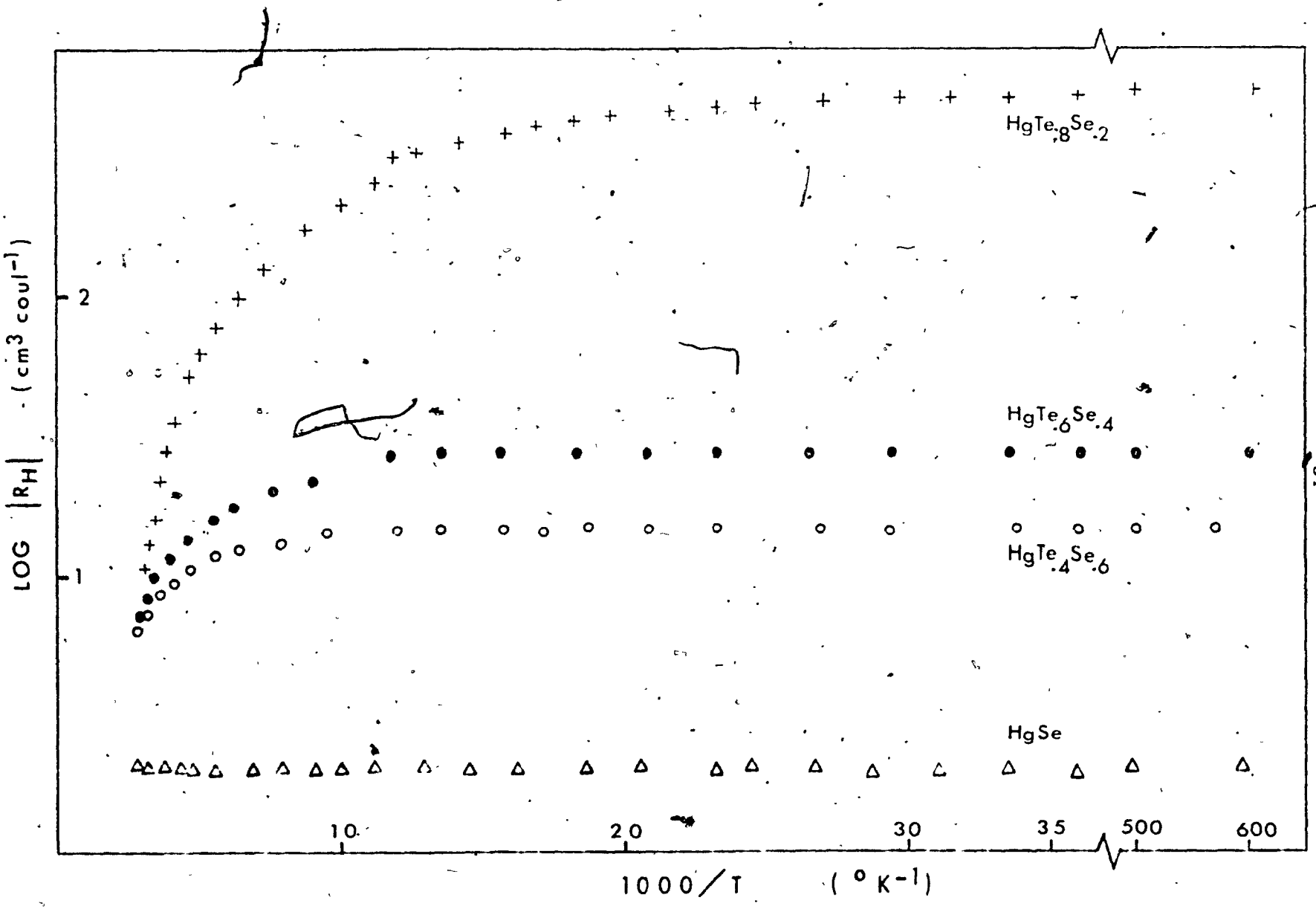

Figure IV-2: Hall Coefficient of HgSe and HgTe-HgSe Alloys as Functions of Temperature

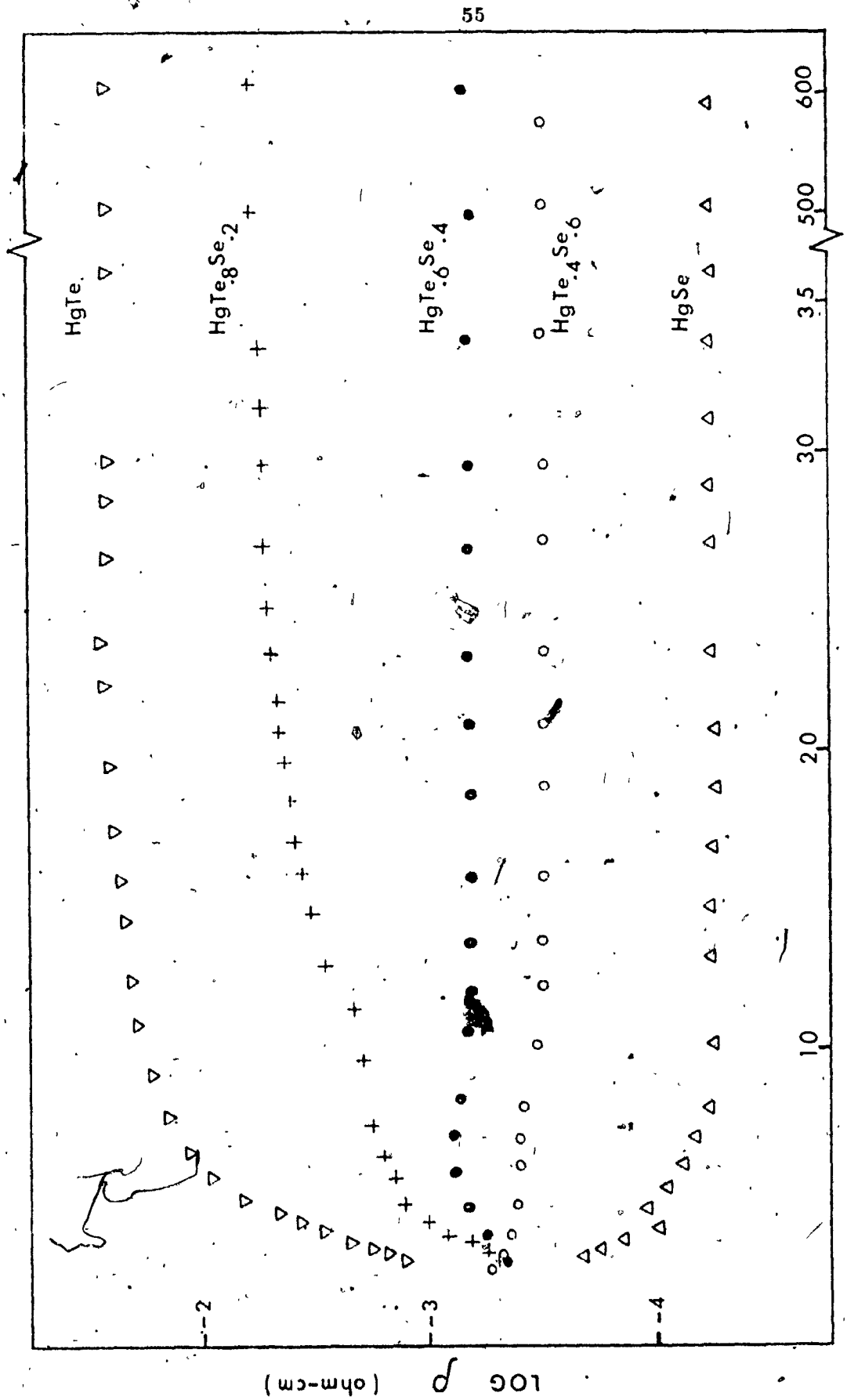

Figure IV-3: Experimental Resistivities of HgTe, HgSe and Their Alloys as Functions of Temperature

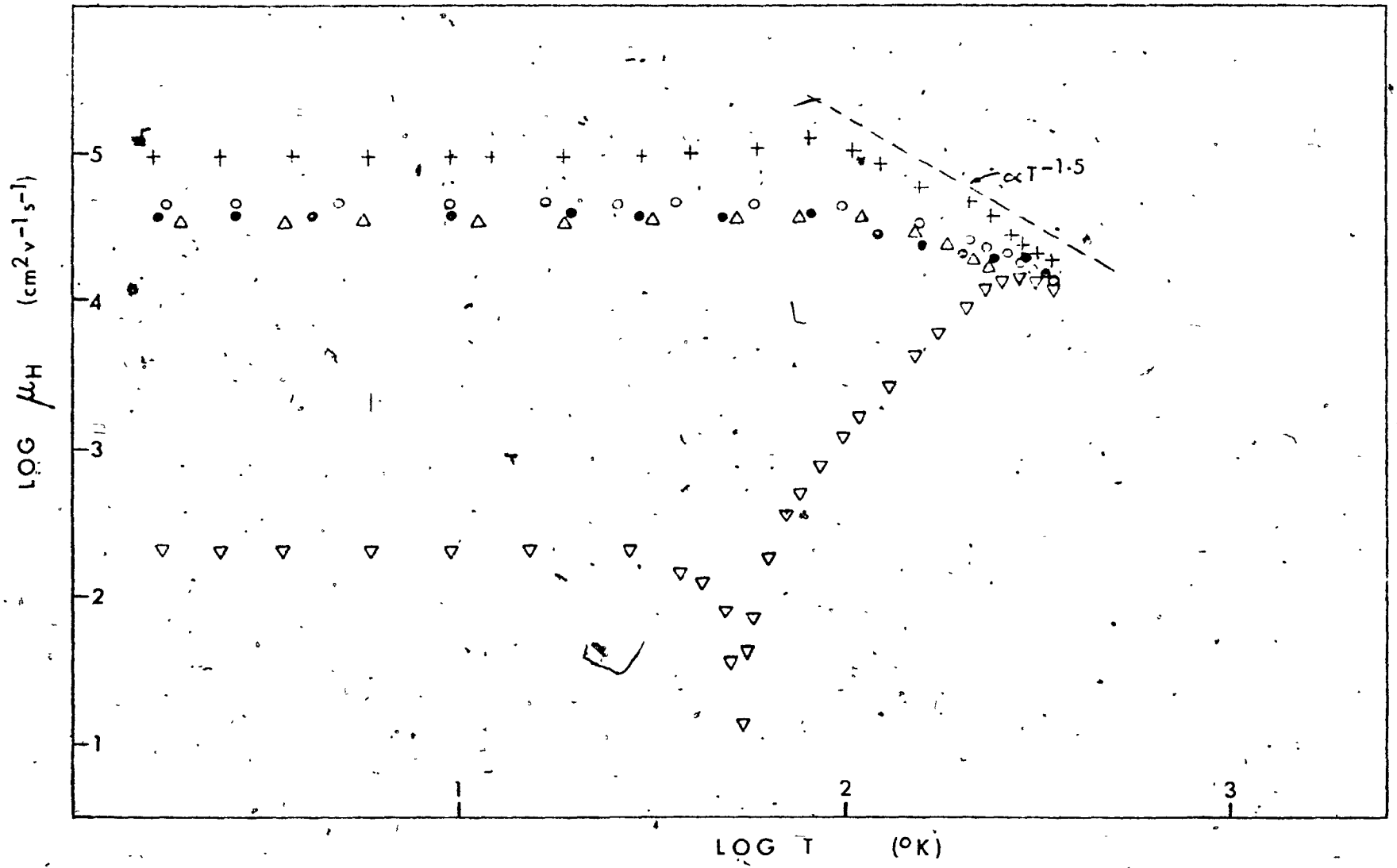

Figure IV-4: Hall Mobilities of HgTe, HgSe and Their Alloys as Functions of Temperature

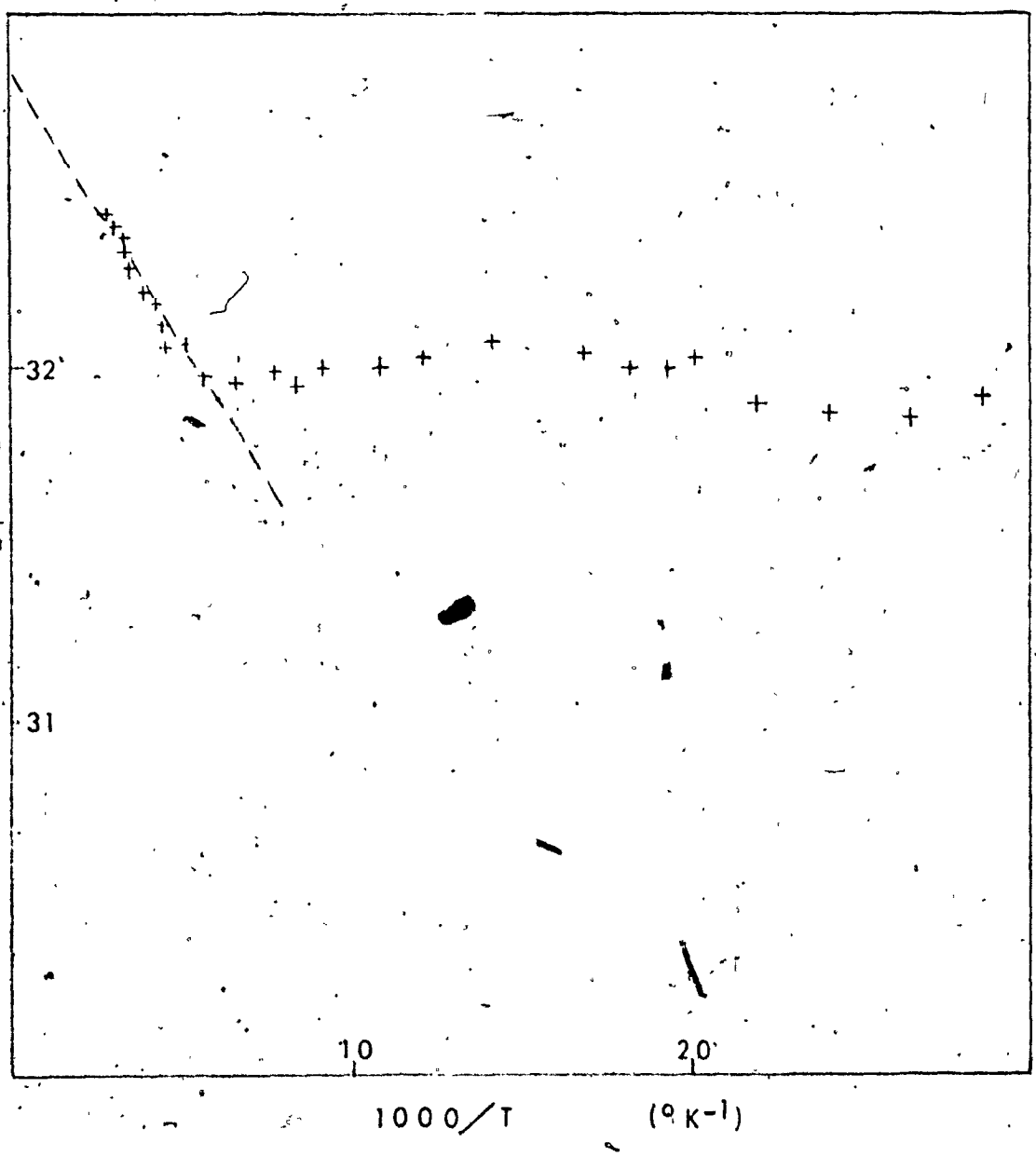

Figure IV-5: Ln $\left[n_i/T^{3/2}\right]$ Versus 1000/T

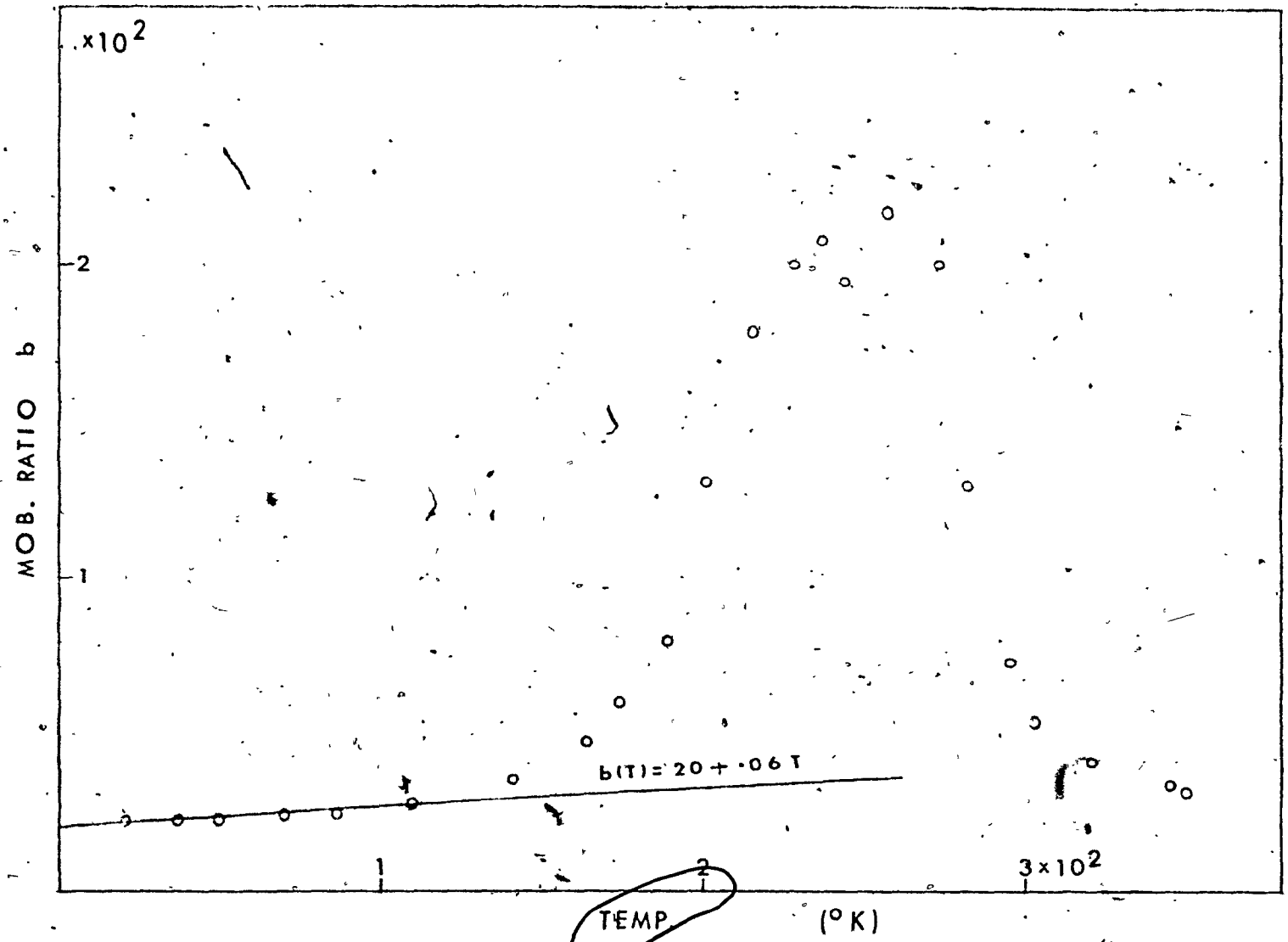

Figure IV-6: Normalized Mobility Ratio Curve of HgTe

CHAPTER V

CONCLUSION

Hall coefficient and electrical resistivity measurements were made on mercury telluride, selenide and their alloys from 1.5°K to 350°K. From the experimental measurements it was found that these compounds have very high electron mobility (in the order of 10^4 cm^2/volt-sec. at room temperature) and the Hall mobility was found to have a $T^{-1.5}$ temperature dependence in the higher temperature range.

It was shown that the conventional two-carrier model fails to describe the properties of HgTe. By using a simple inverted two-carrier model an excellent fit of the p-type experimental Hall coefficient curve of HgTe was obtained. From the result of the analysis it was found that HgTe has the inverted band structure with Γ_8 higher in energy than Γ_6. Also, it was found that the thermal energy gap $E_g = 0 \pm .001$ ev. Results from the analysis of the alloys indicates that the light-hole valence band has to be taken into account. However, this remains to be confirmed by further studies.

On the basis of this work, some recommendations regarding future research on mercury chalcogenides can be made.

By performing Hall coefficient and resistivity measurements as a function of temperature and magnetic field intensity with samples of various impurity concentrations valuable information concerning the mobility and mobility ratio can be obtained. Also, pressure measurements should be made to examine the behaviour of the $\Gamma_8 - \Gamma_6$ energy separation since this would provide information valuable in identifying the band structure of the alloys.

REFERENCE

(1) Black, J., Ku, S. M. and Minden, H. T. "Some Semiconducting Properties of HgTe." Journal of Electrochemical Society, 105, 1958, 723.

(2) Harman, T. C., Logan, M. J. and Goering, H. L. "Preparation Electrical Properties of Mercury Telluride." Journal of Physics and Chemistry of Solids, 7, 1958, 228.

(3) Lawson, W. D., Nielsen, S., Putley, E. H., and Young, A. S. "Preparation and Properties of HgTe and Mixed Crystals of HgTe-CdTe." Journal of Physics and Chemistry of Solids, 9, 1959, 325.

(4) Verie, C., and Decamps, E. Physica Status Solidi, 9, 1965, 797.

(5) Piotrzkowski, R., Porowski, S., Dzinba, Z., Ginter, J., Giriat, W., and Sosnowski, L. "Band Structure of HgTe." Physica Status Solidi, 8, 1965, K135.

(6) Stradling, R. A. "A Millimetre Microwave Determination of the Conduction Band Effective Mass of HgTe." Proceedings of Physical Society, 90, 1967, 175.

(7) Harman, T. C. "Physics and Chemistry of II-VI Compounds." Aven, M. and Prener, J. S., eds. (North Holland Publishing Co., Amsterdam, 1967), Chapter XV.

(8) Groves, S. and Paul, W. "Band Structure of Gray Tin." Physical Review Letters, 11, 1963, 194.

(9) Giriat, W. "On Some Properties of Mercury Chalcogenides." Electron Technology (Warszawa), 4, 1/2, 1971, 37.

(10) Groves, S. H., Brown, R. N. and Pidgeon, C. R. "Interband Magnetoreflection and Band Structure of HgTe." Physical Review, 161, 1967, 779.

(11) Yamamoto, M. "The Shubnikov-de Haas Effect of n-type HgTe." Journal of the Physical Society of Japan, 24, 1968, 73.

(12) Ivanov-Omskii, V. I. "Effective Mass of Holes in Mercury Telluride." Soviet Physics, Semiconductors, 2, 1969, 1122.

(13) Galazka, R. R. and Zakrzewski, T. Physica Status Solidi 23, 1967, K39.

(14) Whitsett, C. R. "Oscillatory Magnetoresistance in Mercury Selenide." Physical Review, 138, 1965, A829.

(15) Harman, T. C. and Strauss, A. J. "Band Structure of HgSe and HgSe-HgTe Alloys." Journal of Applied Physics, 32 (suppl.), 1961, 2265.

(16) Bardeen, J. and Shockley, W. "Deformation Potentials and Mobilities in Non-Polar Crystals." Physical Review, 80, 1950, 72.

(17) Debye, P. P. and Conwell, E. M. "Electrical Properties of n-type Germanium." Physical Review, 93, 1954, 693.

(18) Mansfield, R. "Impurity Scattering in Semi-conductors." Proceedings of Physical Society, B69, 1956, 76.

(19) Erginsoy, D. "Neutral Impurity Scattering in Semiconductors." Physical Review, 79, 1950, 1013.

(20) Kane, E. O. "Band Structure of Indium Antimonide." Journal of Physics and Chemistry of Solids, 1, 1957, 249.

(21) Ehrenreich, H. "Electron Scattering in InSb." Journal of Physics and Chemistry of Solids, 2, 1957, 131.

(22) Harman, T. C., Kleiner, W. H., Strauss, A. J., Wright, G. B., Mavroides, J. G., Houig, J. M. and Dickey, D. H. "Band Structure of HgTe and HgTe-CdTe Alloys." Solid State Communications, 2, 1964, 305.

(23) Groves, S. H. "Recent Experiments on Zero Gap Semiconductors." Proceedings of the Conference of Physics of Semimetals and Narrow-Gap Semiconductors, Texas, 1970. Carter, D. L. and Bate, R. T., eds. (Pergamon Press, New York), 417.

(24) Sniadower, L., Psoda, M. and Galazka, R. R. "X-Ray Measurements of Lattice Dialation in HgTe." Physica Status Solidi, 28, 1968, K121.

(25) Sniadower, L. "Temperature Studies of Magnetoplasma Reflection." Physica Status Solidi, 28, 1968, K125.

(26) Piotrzkowski, R. and Porowski, S. "Temperature Dependence of the Band Structure of HgTe." II-VI Semiconducting Compounds, 1967 International Conference, Thomas, D. G., ed. (W. A. Benjamin, Inc., New York, 1967), 1090.

(27) Zroll, U. Z. Physik, 138, 1954, 167.

(28) Beer, A. C. "Galvanomagnetic Effects in Semiconductors." suppl. 4, Solid State Physics, F. Seitz and D. Turnbull, eds. (Academic Press, New York, 1963).

(29) Van der Pauw, L. J. "A Method of Measuring Specific Resistivity and Hall Effect of Discs of Arbitrary Shape." Philips Research Report, 13, 1958, 1.

(30) ASTM. "Standard Method for Measuring Hall Mobility in Extrinsic Semiconductor Single Crystals." F76-68.

(31) Herring, C., Geballe, T. H. and Kunzlar, J. E. Bell System Technical Journal, 38, 1959, 657.

(32) Long, D. and Myers, J. Physical review, 120, 1960, 39.

(33) Nielson, S. "Reaction of Indium Solder with HgTe." British Journal of Applied Physics, 10, 1959, 380.

(34) Krawczyniuk, R. "Digital Computer Control of Resistivity and Hall Measurements of Semiconductor." M.Sc. 1971, Sir George Williams University.

(35) Smith, R. A. "Semiconductors." Cambridge University Press, 1959, 187.

(36) Rodot, M., Rodot, H. and Triboulet, R. "Some Properties of HgSe-HgTe Solid Solutions." Journal of Applied Physics, 32 (suppl.), 1961, 2254.

(37) Gobrecht, H., Gerhardt, U., Peinemann, B. and Tausend, A. "Electrical and Optical Properties of Mercury Selenide (HgSe)." Journal of Applied Physics, 32 (suppl.), 1961, 2246.

(38) Putley, E.H. "The Hall Effect and Related Phenomena." Butterworth & Co., 1960, Chapter IV.

(39) Galazka, R. R. "Temperature Dependence of Intrinsic Concentration in HgTe." Physics Letters, 32A, 1970, 101.

(40) Dingle, R. B. "The Fermi-Dirac Integrals." Applied Science Research, B6, 1956, 225.

APPENDIX

PROGRAM LASTIME

This computer program is written in Fortran IV language primarily to generate the carrier concentrations required in the analysis of Hall coefficients of mercury chalcogenides using the inverted two-carrier model as described in section 4.22. The listing of the program is given below.

Worth mentioning is the external function subprogram, Function Fermi, because of the importance of the Fermi Integral in semiconductor physics. The integrals are generated using equations (7), (9), (21) and (24) of Dingle's work (40).

```
PROGRAM
```

```
      GO TO 100
140   IF(X.LT.0.001) GO TO 200
      C=ABS(X-X1)
      IF((Y-0.0001).LT.Y1) GO TO 150
      CO...=[illegible]
      FCN=K(N...)
150   FCN=FCN*1.0
      PCN=[illegible] (X-X1)*FCN
      IF(PCN.LT..0005) PCN=0.0005
160   E1=E1+FCN*CO
      X1=X
      Y1=Y
      GO TO 100
200   EF=E1*[illegible]
      T1000=1000./T
      [illegible]
      [illegible]
      [illegible]=([illegible]+1./(NN+E)))/(NN+N)
      [illegible]
      IF([illegible]) [illegible]
      S1=([illegible])/[illegible]
      [illegible]
      PRINT [illegible] T1000,T [illegible]
      FORMAT([illegible]A,[illegible]5.4,2F11.5)
      [illegible]
      PRINT [illegible] T1000
      FORMAT([illegible]5A,F15.4)
      [illegible]
      END
```

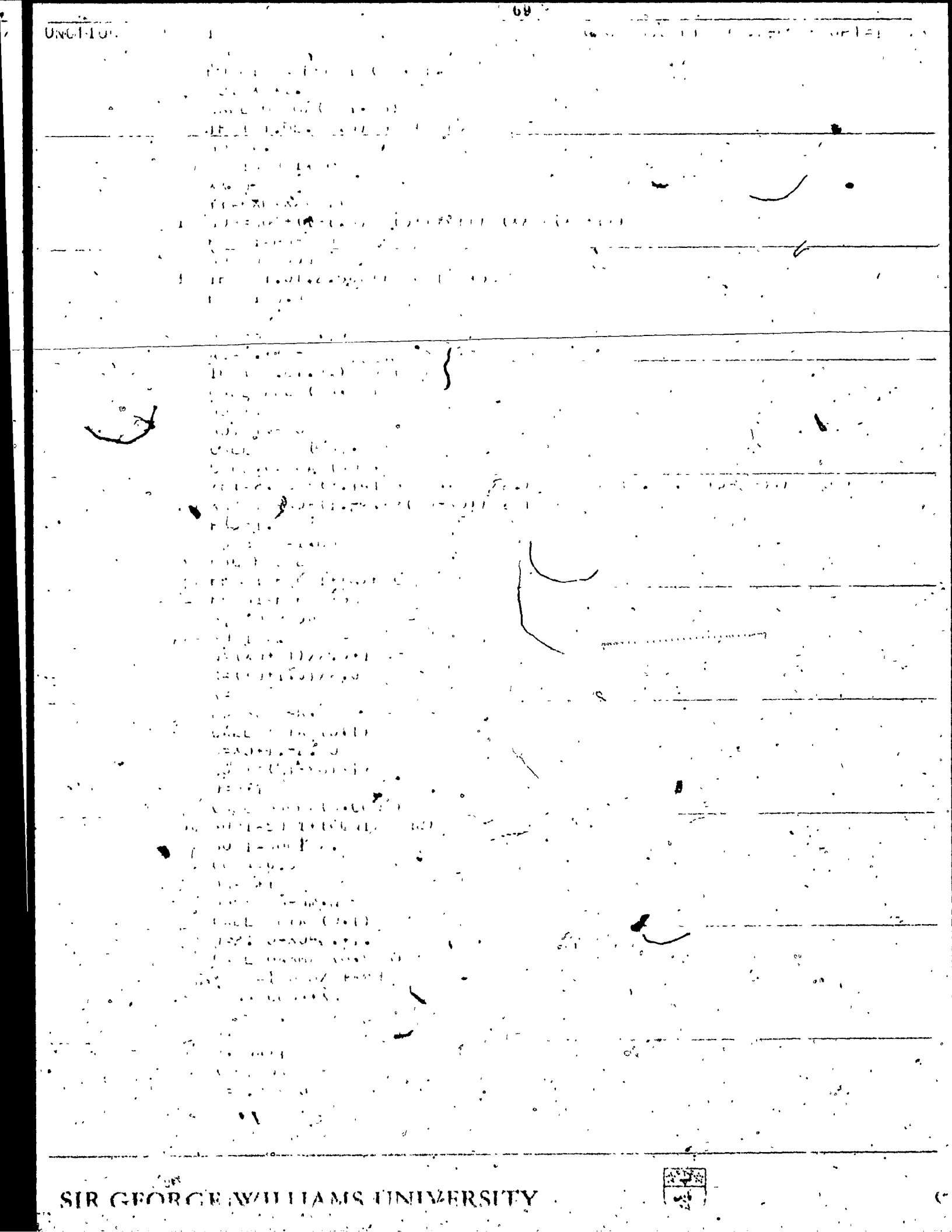

UNCTION [illegible]

[illegible]

JBROUTINE [illegible]

```
IF [illegible]
```

```
SUBROUTINE
```

```
SUBROUTINE
```

```
SUBROUTINE
```